DESIGN AND EXPERIMENTAL STUDY OF HYDROSTATIC THRUST AIR FOIL BEARING

by

MYONGSOK SONG

Presented to the Faculty of the Graduate School of

The University of Texas at Arlington in Partial Fulfillment

of the Requirements

for the Degree of

MASTER OF SCIENCE IN MECHANICAL ENGINEERING

THE UNIVERSITY OF TEXAS AT ARLINGTON

MAY 2018

Acknowledgments

I would like to take this opportunity to express appreciation to academic advisor, Dr. Daejong Kim, for whom I have the utmost respect. He has helped to guide me, and I am forever grateful. I also want to show my gratitude to Dr. Hyejin Moon & Dr. Andrey Bayle for serving as committee members.

I give sincere thanks to Kermit Beird and Sam Williams from the machine shop for always helping me. Thanks also go to the members of the Turbo Machinery and Energy Systems Laboratory for their friendship and guidance.

I would like to thank Srikanth Hanovara-Prasad, Amirreza Niazmand, Nguyen Thao Latray, Vaibhav Indulkar, Behzad Zamanian Yazdi, Sri Ram Gaddameedi, Liu Wanhui and all colleagues at Turbomachinery Energy System Laboratory for their guidance and support.

Finally, I would like to thank my family. I cannot imagine whom or where I would be if I had not always been able to count on not only their financial support but also continuous encouragement during studies.

May 22, 2018

Abstract

DESIGN AND EXPERIMENTAL STUDY ON HYDROSTATIC
THRUST AIR FOIL BEARING

Myongsok Song, MS

The University of Texas at Arlington, 2018

Supervising Professor: Daejong Kim

Oil-free bearing technology has several advantages over conventional oil-lubricated bearings. These advantages include high-speed operation, reduced weight, and increased reliability. Consequently, oil-free technology is expected to replace conventional bearings in a variety of applications. However, many challenges need to be addressed for widespread adoption of oil-free technology such as lower load capacity during start/stop and issues with controlling temperature.

Thrust bearings, unlike their radial counterparts, are used for supporting axial loads and have become more important in recent years because of layout requirements other than double overhang configuration gaining consideration for specialized applications. Moreover, the requirements are demanding more extreme condition such as higher load capacity and temperature management.

To address the challenge of listed problems, a new hydrostatic type of the thrust air foil bearing with 154mm outer diameter is introduced. Pressurized air is injected through 32 orifices which enable not only higher load carrying capacity during start/stop but also enhanced thermal management because of cooling effect.

The test result of flat air bearing, damaged air foil bearing, and simple theoretical result will be shown and compared with the experimental results. The load capacity of the

hydrostatic thrust foil bearing was found to be 1.5 kN (static), and it has an meaningful improvement compare to hydrodynamic and hydrostatic flat air bearing.

Due to the experiment, this approach of hydrostatic air foil thrust bearings can be used extensively in the turbomachinery area without using oil under heavy load and high-temperature situation.

Nomenclature

C_{Th}	Bearing Clearance
D	Diameter
D_i	Inner Diameter
D_o	Outer Diameter
D_h	Orifice Diameter
F	Applied Load
N	Revolutions per minute (RPM)
P	Pressure
P_a	Ambient Pressure
P_{avg}	Average Pressure
P_i	Inlet Pressure
P_s	Supply Pressure
R	Radius
R_i	Inner Radius
R_o	Outer Radius
RPM	Revolution per minute
D_h	Orifice Diameter
$\vec{V}$	Velocity
h	Film thickness in mathematical model
u, v, w	Flow speeds within the film
$U1, V1, W1, U2, V2, W2$	Surface speeds in mathematical model
(x, y, z)	Orthogonal coordinate axes in mathematical model
Π	Mathematical Constant; the ratio of a circle's circumference to its diameter

ρ	Density
η	Fluid viscosity
μ	Dynamic Viscosity
$\mu_{friction}$	Friction Coefficient
ω	Angular Velocity

Table of Contents

List of Illustrations

List of Tables

Chapter 1

Introduction

Bearings are machine elements that allow components to move with respect to each other, and they play an essential role in turbomachinery systems. Their function is to support a shaft in the axial or radial direction due to loading from compressor, turbine and other components connected to the shaft. Bearings in various forms and for various applications have been used since ancient times. However, in recent years, their importance has increased as machines have been driven to higher power and speeds. Several different types of the bearing are classified in Figure 1-1 and explained in this chapter.

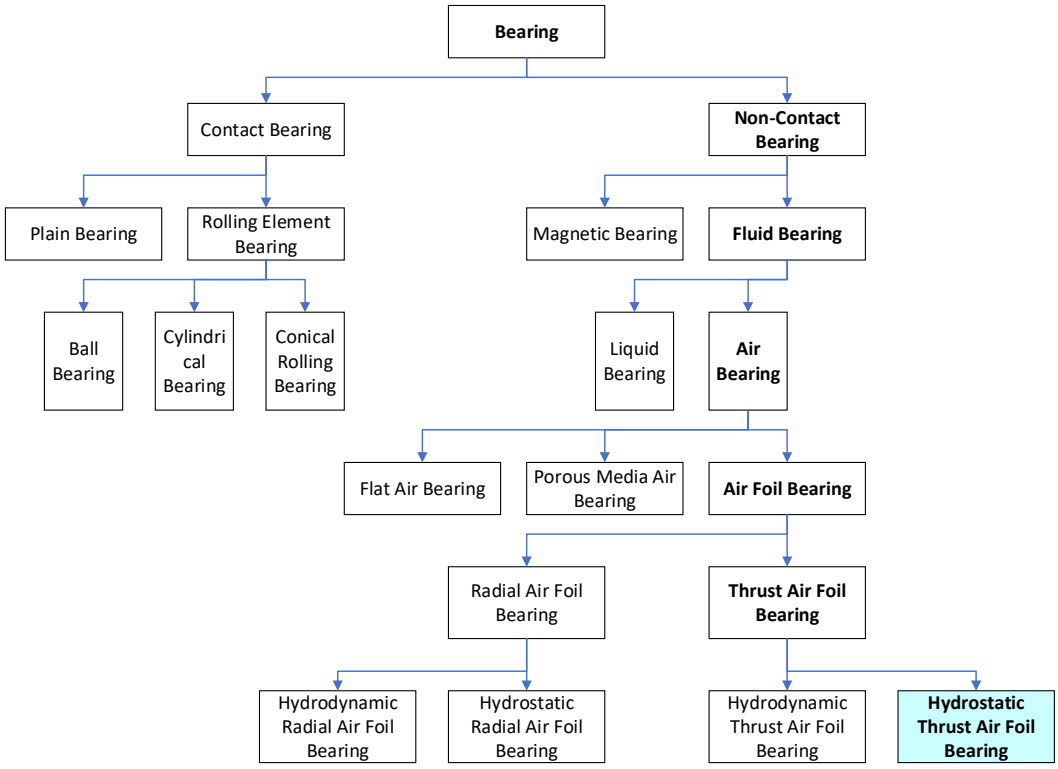

Figure 1-1 Classification of Bearing

Bearings are broadly classified as contact and non-contact bearings depending on the contact type. Contact bearings have mechanical contact between elements, and they include sliding, rolling and flexural bearings. Mechanical contact brings high stiffness normal to the direction of motion, but wear or fatigue limit the bearing's lifetime. Plain bearings and rolling elements bearings are representative of contact bearings. Non-contact bearings are largely categorized into fluid film bearings (liquid and air bearings such as flat air bearing, porous media bearing, air foil bearing) and magnetic. They are operated through the presence of a fluid film in the bearing or through magnetic levitation of the shaft above the bearing. This lack of mechanical contact means that friction can be eliminated. However, viscous drag still occurs when fluid is present. Despite the presence of viscous drag, they are capable of operating at higher speeds and have virtually infinite service lives if the external power units required to operate them do not fail.

Plain bearings, also known as bushes, bushings or sleeve bearings, are the simplest and most compact type of contact bearing. It is composed only of a bearing surface and no moving parts. A typical example of a plain bearing is simply a shaft rotating in a sleeve. The bearing performance is dependent on the material selection and the operating condition, a variety of low friction material and solid lubricant are researched applied in plain bearings.

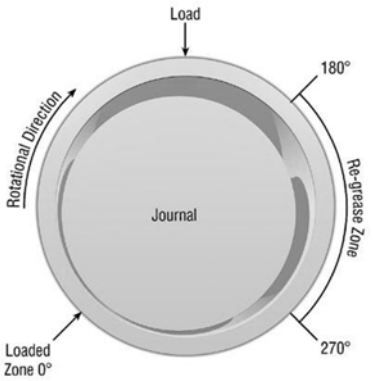

Figure 1-2 Structure of the plain journal bearing [1]

Rolling element bearings are widely used and well-known contact bearings. Prominent rolling element bearings include ball bearings, cylindrical bearings, and conical rolling bearings. Figure 1-3 shows the structure of a typical ball bearing design, and it comprises rolling bearings, supporting cage, inner race, and outer race. During the operation of rolling bearings, the outer race stays stationary while the inner race rotates with the shaft.

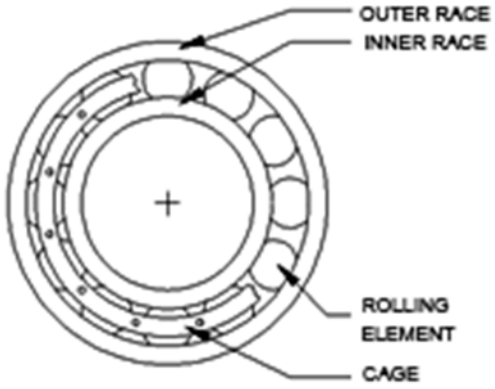

Figure 1-3 Structure of the Ball Bearing [2]

Regarding the wear issue, rolling element bearings have better advantages than plain bearings because they have point or line contact between surfaces. However, the performance and lifetime of these bearings are limited by the rotating speed because of friction. The rolling element bearings can undergo deformation such as brinelling which is the indentation caused by excessive loading on the rolling elements.

Magnetic bearings are a type of non- contact bearings that support a load using magnetic levitation. Figure 1-4 shows a design and operating principle of the magnetic bearings. The gap sensors measure the displacement between the rotating shaft based on the reference position. The controller provides a feedback control signal from the

measurement data, and the power amplifiers convert the signal to a current which controls the rotor.

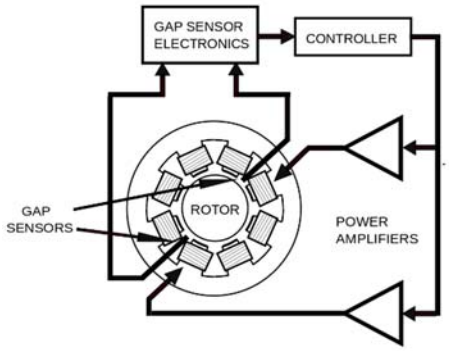

Figure 1-4 Structure of Magnetic Bearing [3]

Fluid bearings are a class of non-contact bearings in which the load is supported by a pressurized liquid or air film between the bearing surfaces. Since there is no mechanical contact between the moving parts, they have lower friction, wear and vibration than contact type of bearings even at high speeds. For example, fluid bearings used in hard disk drive spindle motor barely makes any noise even at 5000 rpm.

A variety of fluids can be used in fluid film bearings including liquid or air. Liquid bearings have higher viscosity and therefore have a high load capacity compared to air bearings. However, the high viscosity also results in higher frictional losses in comparison to air bearings.

Fluid film bearings are further classified into self-acting bearings (hydrodynamic) and externally pressurized bearings (hydrostatic). The fluid bearings also can be divided into radial and thrust type depending on the loading mechanism.

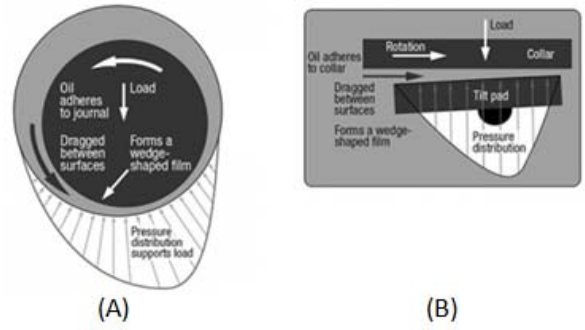

Figure 1-5 Various Form of Fluid Bearing 2 (A) Radial Type (B) Thrust Type [4]

Air Foil bearings are a class of air bearings in which the hydrodynamic film is formed between a compliant support structure and the rotating shaft. As seen in Figure 1-6, air foil bearings consist of the top foils and the corrugated bump foils. Once the shaft rotates fast enough, the air film generated by the pressure pushes the foil away from the shaft, so it is contactless. Like other fluid type bearings, the air foil bearings have radial type (supporting radial loads) or thrust type design (supporting axial loads), and it is shown in Figure 1-6.

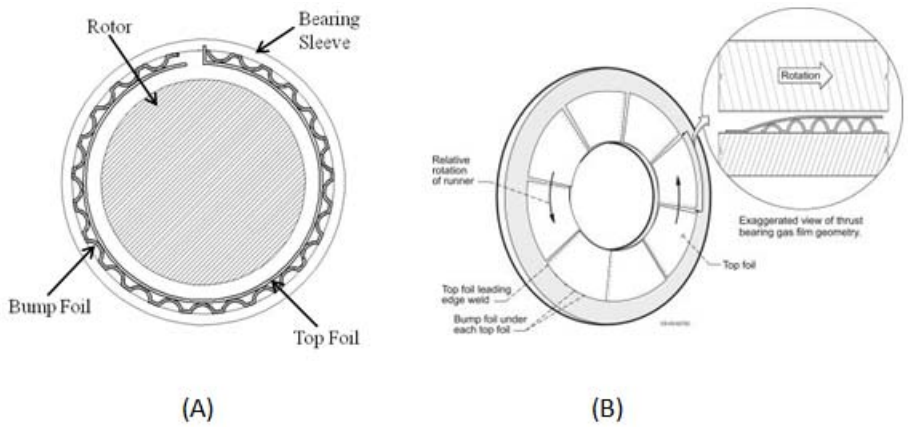

Figure 1-6 Various Form of Air Foil Bearing (A) Radial Type (B) Thrust Type [5]

The several advantages of the air foil bearings come from the removal of the oil systems required by traditional bearing designs, and they are shown in Table 1-1.

Table 1-1 Advantages of Air Foil Bearing [6]

Higher efficiency	Lower Friction
Low Maintenance	Oil-free Operation.
Soft Failure	Bearing is sacrificed without damaging other components
Environmental Durability	No degradation of lubricant due to operating conditions.
High-Speed Operation	Low viscosity
Thermal stability of working fluid	Gas properties remain constant over a wide temperature range.

Since the first air foil bearing design was introduced in 1960's by Garrett AiResearch (now Allied Signal), they have been widely used from microturbine to air cycle machines used for aircraft. The air foil bearings are recognized as promising technologies in the turbomachinery area.

However, the most popular cases of foil bearing technology, studied and applied, have been the hydrodynamic type of bearing due to its lightweight and simple design, and they have operating limitations in carrying a higher load during start/stop. Therefore, the current research of the foil bearing technology is mainly focused on solving disadvantages, such as using external pressure for supply air film in the bearing (hydrostatic design).

Chapter 2

Literature Review

Since the first compliant foil bearing was introduced by Block and Van Rossum in 1953, air foil bearing technology is successfully developed and deployed in turbomachinery area, such as from microturbines to aircraft air cycle machines [7]. This is because air foil bearing technology conforms most of the requirements of efficient oil-free turbomachinery area by increasing load capacity and reliability.

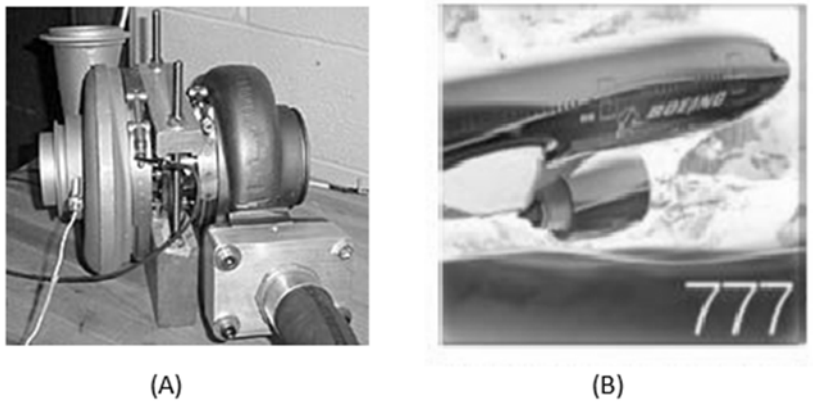

(A) (B)

Figure 2-2-1 (A) High Speed Microturbine with Air Foil Bearings

(B) Boeing 777 incopating Air Foil Bearings

In recent years, the research has been geared towards either improving features like load capacity, damping capacity and stability or developing novel methodologies for bearing performance estimation. Based on available experimental data, DellaCorte et al. proposed a semi-empirical relationship for a load capacity of a radial foil bearing [8]. Similar relations were developed for stiffness and damping coefficients of radial foil bearings [9] [10].Other researchers developed scaling relationships to estimate clearance and stiffness of radial foil bearings [11] [12]. Many researchers have studied the performance and failure

of radial foil bearings [13] [14] [15]. However, the literature on the foil thrust bearings is not as plentiful.

The axial loads in turbomachinery systems were not a major concern in the past as opposite impellers were used to minimize thrust loading. However, demands for increased speed, power and size restrictions have resulted in the exploration of new layouts which include single impeller and corresponding higher thrust loads. In 1983, Heshmat et al. employed equivalent foundation model for evaluating the static performance of foil thrust bearings [16]. Their simulation did not consider the effect of top foil deflection. In 1999, Iordanoff developed a design method for foil thrust bearings considering simplified structural analysis [17]. The method was employed to design an 80 mm OD and 40 mm ID thrust bearing. Heshmat et al. conducted experiments with anti-wear coatings to evaluate the performance of foil bearings [18]. San Andres and Ryu predict static and dynamic forced response of thrust air foil bearings by using computational model [19]. Peng and Khonsari employed numerical methods for predicting load capacity of foil bearings [20] [21]. Ravi kumar et al. designed thrust bearing test rig with cascaded air foils up to 45000 rpm and obtained the relationship between load-carrying capacity and the function of different geometric and operating parameters [22].

Hydrostatic types of air foil bearings have also been researched to improve the bearing performance in recent years. Kim and Park designed, constructed and tested the first hydrostatic air foil bearing with compression springs as an elastic foundation. The bearing showed higher load capacity than a hydrodynamic bearing. Further, the start torque was comparable to friction torque during steady-state hydrodynamic operation [23]. Manish et al. extended the work in a paper by using support structure made of corrugated bump foils. This bearing was designed with higher structural stiffness than the first design. Also, a new test rig was constructed to analyze the load capacity of the bearing at higher

speeds. The results showed that the performance of the hydrostatic air foil bearing with bump foil support structure had similar load capacity at high-speed operation compared to hydrodynamic bearing due to the dominant hydrodynamic effect at high speeds [24]. However, the hydrostatic bearing showed improved load capacity at low speed due to the hydrostatic pressurization.

For hydrostatic air foil thrust bearing, NASA designed hydrostatic thrust air foil bearing with 100mm and showed data for improving bearing characteristics in 2005. [25] Lee and Kim predicted the performance hydrostatic air foil thrust bearings by using physical analysis and computer simulation. The result shown that hydrostatic case can make thicker air film than hydrodynamic case, and it shows hydrostatic type can also bring more benefits in thrust foil bearing such as increase load capacity and protect wear issues [26].

Chapter 3

Research Objective

Air foils bearings have numerous advantages as described in the previous chapter. However, there are challenges that need to be addressed. These bearings are limited by lower load capacity during start/stop. Use of hydrostatic foil bearing can address this issue. Further, thrust foil bearings have received limited attention in the past. However, due to existing need for better thrust bearings, this thesis focuses on hydrostatic thrust foil bearings.

The objective of the current research is to design a thrust foil bearing that can support 1.5 kN axial load. The designed thrust foil bearing is evaluated for load capacity by the construction of a test rig.

The axial load on the bearing is applied through a pneumatic actuator and the load capacity is evaluated based on the response observed due to friction torque. The load on the bearing is determined to be the bearing load capacity when the friction torque rises sharply. Mass flow controllers are used for controlling air supply to bearing and the actuator. Proximity sensors are used for determining displacement of the thrust runner and the bearing back plate.

Chapter 4

Theoretical Background

4.1 Governing equation

Fluid bearings, including air foil bearings, are non-contact bearings that utilize a thin film of pressurized gas to provide a low friction interface between two closely spaced surfaces.

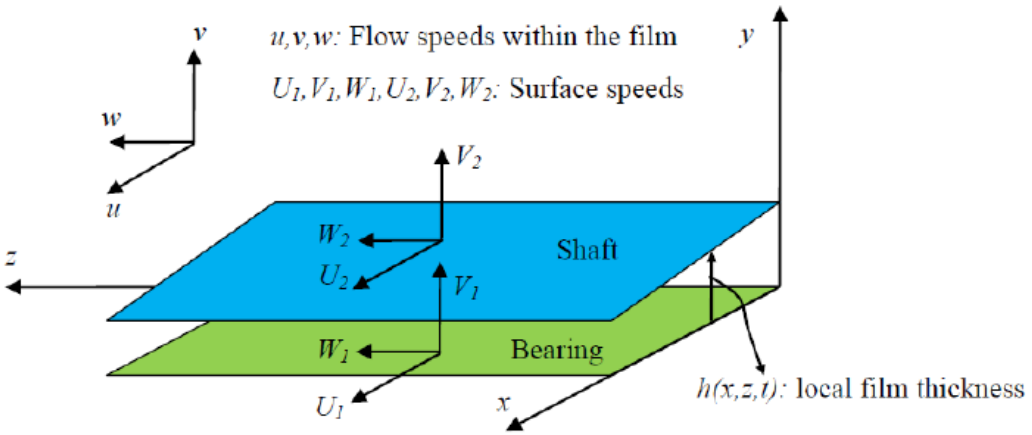

Figure 4-1 Geometry of Fluid Thin Film [27]

The surfaces usually shape a converging gap, and it results in the pressure generation.

A geometry based on the Cartesian coordinate system is shown In Figure 4-1. $U1, V1\ and\ W1$ denote velocities of stationery surface in $x, y\ and\ z$ directions, respectively, and $U2, V2\ and\ W2$ denote velocities of moving surface in $x, y\ and\ z$ directions, respectively.

The Reynolds Equation is a partial differential equation governing the most fluid bearing system in classical lubrication theory. The equation is based on the typical assumption of negligible flow inertia (low Reynolds numbers), this film (negligible curvature effect), and incompressible flow, and it can be derived from the Navier-Stokes equation. The derivation procedure of the classical lubrication theory is briefly repeated here.

Mass continuity equation:

$$\frac{\partial \rho}{\partial t}+\frac{\partial \rho u}{\partial x}+\frac{\partial \rho v}{\partial y}+\frac{\partial \rho w}{\partial z}=0 \tag{1}$$

In incompressible, fluid, the continuity equation is simplified to;

$$\frac{\partial u}{\partial x}+\frac{\partial v}{\partial y}+\frac{\partial w}{\partial z}=\nabla \cdot \vec{V}=0 \tag{2}$$

Momentum Equation also can be simplified to;

$$\rho\left(\frac{\partial u}{\partial t}+u\frac{\partial u}{\partial x}+v\frac{\partial u}{\partial y}+w\frac{\partial u}{\partial z}\right)=-\frac{\partial p}{\partial x}+\mu\left(\frac{\partial^2 u}{\partial x^2}+\frac{\partial^2 u}{\partial y^2}+\frac{\partial^2 u}{\partial z^2}\right) \tag{3}$$

$$\rho\left(\frac{\partial v}{\partial t}+u\frac{\partial v}{\partial x}+v\frac{\partial v}{\partial y}+w\frac{\partial v}{\partial z}\right)=-\frac{\partial p}{\partial y}+\mu\left(\frac{\partial^2 v}{\partial x^2}+\frac{\partial^2 v}{\partial y^2}+\frac{\partial^2 v}{\partial z^2}\right)$$

$$\rho\left(\frac{\partial w}{\partial t}+u\frac{\partial w}{\partial x}+v\frac{\partial w}{\partial y}+w\frac{\partial w}{\partial z}\right)=-\frac{\partial p}{\partial z}+\mu\left(\frac{\partial^2 w}{\partial x^2}+\frac{\partial^2 w}{\partial y^2}+\frac{\partial^2 w}{\partial z^2}\right)$$

When the assumptions from the fluid film geometry are applied in (3), we can get more simplified equations;

$$\frac{\partial p}{\partial x}=\mu\frac{\partial^2 u}{\partial y^2} \tag{4}$$

$$\frac{\partial p}{\partial z}=\mu\frac{\partial^2 w}{\partial y^2}$$

Since the pressure gradient terms do not change across the thickness h, the equations (4) can be integrated two times based on the following boundary conditions as follows;

$$u(0)=U_1 \tag{5}$$

$$u(h)=U_2$$

$$w(0)=0$$

$$w(h)=0$$

The following equation is derived, and we can solve for u and w;

$$u=\frac{1}{2\mu}\frac{\partial p}{\partial x}(y^2-yh)+\left(1-\frac{y}{h}\right)U_1+\frac{y}{h}U_2 \tag{6}$$

$$w = \frac{1}{2\mu}\frac{\partial p}{\partial x}(y^2 - yh)$$

Now, since both *p* and *v* are an unknown value, *u* and *w* cannot be plugged and integrated into the equation of continuity. This issue can be solved by averaging *v* over the thickness *h* and integrating all other terms in the equation with respect to *y*. This gives;

$$[v]_0^{y=h(x,t)} = -\int_0^{h(x,t)} \frac{\partial u}{\partial x} dy - \int_0^{h(x,t)} \frac{\partial w}{\partial z} dy \tag{7}$$

Therefore, the averaged velocity across the thickness can be presented as follows;

$$[v]_0^{y=h(x,t)} = -(V_1 - V_2) = \frac{dh}{dt} \tag{8}$$

Finally, values for *u* and *w* can be plugged and integrated. After some simplification, the generalized Reynolds Equation is derived as follows;

$$\frac{\partial}{\partial x}\left(\frac{h^3}{\eta}\frac{\partial p}{\partial x}\right) + \frac{\partial}{\partial y}\left(\frac{h^3}{\eta}\frac{\partial p}{\partial y}\right) = 6h\frac{\partial}{\partial x}(U_1 + U_2)h + 6(U_1 - U_2)\frac{\partial h}{\partial x} + 12\frac{\partial h}{\partial t} \tag{9}$$

Where

$$h = Film\ thickness \tag{10}$$

$$\eta = Fluid\ viscosity$$

$$U_i = Velocity\ at\ boundary\ (with\ respect\ to\ x)$$

$$V_i = Velocity\ at\ boundary\ (with\ respect\ to\ x)$$

$$P = Pressure$$

$$z = direction\ of\ the\ height$$

The generalized Reynolds equation as above shows the mathematical statement of the classical theory of lubrication. Physically, it can be thought of as expression of conservation principles for a system made up of fluid flow between two surfaces.

The left-hand side terms of the equation show fluid flow due to pressure gradients across the domain, while the right-hand side terms represent flow induced by movements of the bounding

surfaces and shear-induced flow by the sliding velocities U and V. From the equation, neither such motions of the bounding surfaces or no time dependence can be assumed.

4.2 Pressure Profile

Knowing the pressure profile is important in air foil bearing systems because load capacity depends on the pressure of the air film. Specifically, it can be more important in hydrostatic thrust air foil nearing systems because controlled inlet pressure can improve load carrying capacity.

In this chapter, simple method to calculate pressure profile is explained. Figure 4-2 and Figure 4-3 shows the geometry and theoretical pressure distribution for a thrust flat air bearing with a single hole. At the perimeter of the bearing, the pressure is equal to the ambient pressure P_a and at the center, within the limits of orifice diameter D_h; the pressure is equal to the inlet pressure P_i. P_i is determined by the pressure from the back side (source pressure) P_s, it can be roughly calculated at half of the supply pressure ($\frac{P_s}{2}$). In order to use these boundary conditions, a value of D_h must be known. For simple calculation, average pressure distribution can be easily calculated at $\frac{P_a+P_i}{2}$ by using triangle rooftop pressure distribution model. Load carrying capacity also can be calculated by multiplying contact area (A).

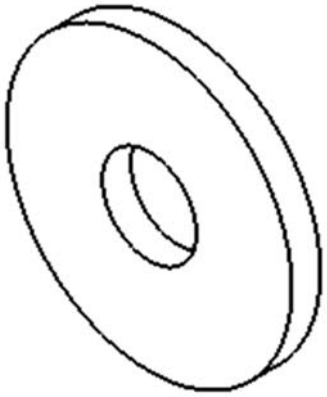

Figure 4-2 Topside of Flat Air Thrust Bearing with Single Orifice

With Outer Diameter (D_o) and Orifice Diameter (D_h) noted.

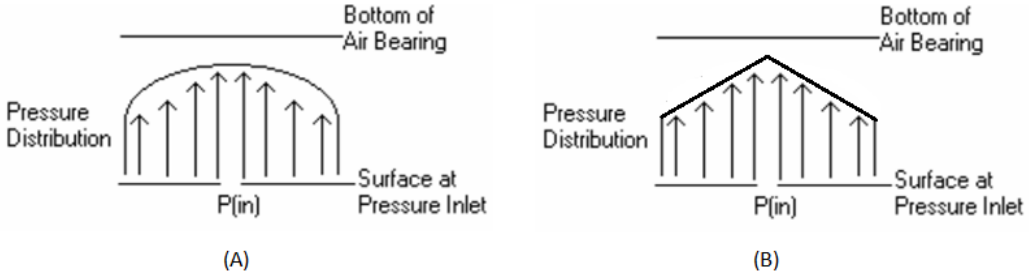

Figure 4-3 Theoretical Pressure Distribution for Flat Air Thrust Bearing with Single Orifice

(A) Parabolic Rooftop Distribution Model (B) Triangle Rooftop Distribution Model

<Equation for Flat Air Bearing with Single Orifice> (11)

$$Average\ Pressure:\ P_{avg} = \frac{P_a + P_i}{2}$$

$$Contact\ Area:\ A = \frac{\pi}{4}\left({D_o}^2 - {D_h}^2\right)$$

$$Load\ Capacity:\ F = (P_{avg} - P_a) \cdot A$$
$$= \left(\frac{P_a + P_i}{2} - P_a\right) \cdot \frac{\pi}{4}\left({D_o}^2 - {D_h}^2\right)$$

For a thrust flat air bearing with double grooves, the geometry has a donut shape with circular grooves . Figure 4-5 and Figure 4-5 shows the geometry and cross-section pressure distribution for the thrust flat air bearing with the double grooves. In this case, trapezoidal rooftop model is applied for pressure profile calculation which is based on triangle model. At the outer diameter and inlet diameter, both pressure is equal to the ambient pressure P_a and at the center of the orifices, the pressure is equal to the inlet pressure P_i. The inlet pressure P_i also can be derived by half of the supply pressure P_s as well.

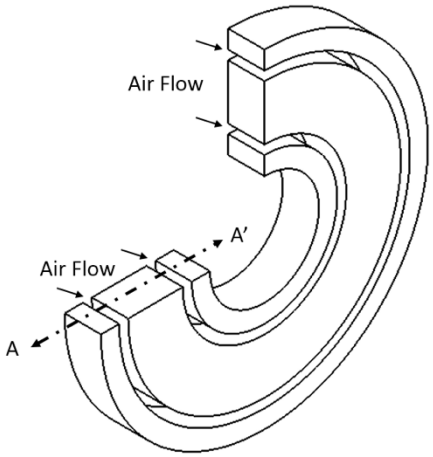

Figure 4-4 Geometry of Thrust Flat Air Bearing with Double Grooves

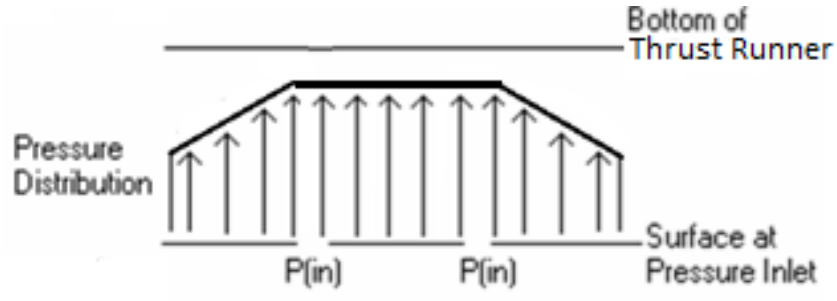

Figure 4-5 Pressure distribution for Flat Air Bearing with Double Grooves

(Cross section AA')

In order to use these boundary conditions, a value of hole diameter must be known. Average pressure can be easily calculated at the shape of the pressure profile divided by $\frac{P_a+P_i}{2}$ by using triangle rooftop pressure distribution model. Load carrying capacity also can be calculated at shape of the pressure profile multiplied by $\frac{P_a+P_i}{2}$.

< Equation for Thrust Flat Air Bearing with double grooves> (12)

$$Inner\ Diameter = D_i, \quad Outer\ Diameter = D_o\ ,$$
$$Orifice\ Diameter = D_h$$

$$Contact\ Area:\ A = \frac{\pi}{4}\left[\left({D_o}^2 - {D_i}^2\right) - 32 \cdot {D_h}^2\right] \approx \frac{\pi}{4}\left({D_o}^2 - {D_i}^2\right)$$

$$Average\ Pressure:\ P_{avg} = \frac{Tripezodal\ Pressure\ Area}{D_o - D_i}$$

$$Load\ Capacity:\ F = \left(P_{avg} - P_a\right) \cdot A$$

However, applying this equation is available only for certain types of flat air bearing; they are not suitable for hydrostatic thrust air foil bearing, because of exiting many other variables such as hydrodynamic effect.

4.3 Power Loss Calculation

If no heat loss by the foil bearing system is assumed, the power loss could be calculated as follows.

$$P_{Loss,TH} = \omega\tau_{Loss,TH} \quad (13)$$

$$P_{Loss,TH} = \omega\tau_{Loss,TH} = \omega \int_0^{2\pi} \int_{R_i}^{R_0} r^2 \left(\frac{h}{2}\frac{dp}{rd\theta} + \frac{\mu d\omega}{h}\right) d\theta dr \tag{14}$$

$$= N\frac{2\pi}{60}\int_0^{2\pi} \int_{R_i}^{R_0} \left(r\frac{h}{2}\frac{dp}{d\theta}\right) d\theta dr + N^2\mu(\frac{2\pi}{60})^2 \int_0^{2\pi} \int_{R_i}^{R_o} (\frac{r^3}{h}) d\theta dr$$

The first term in (14) is from pressure gradient between the film (less than 5%), and the second term is because of the shear stress which is dominant. Ignore the first term and calculate the second term, the power loss can be explained as below.

$$P_{Loss,TH} \approx \mu N^2 \frac{{R_o}^4 - {R_i}^4}{C_{Th}} \tag{15}$$

In runner side, we can measure torque loss based on the applying load from the experimental data, and the torque value can be plugged the equation as follows.

$$\tau_{Loss,TH} = \frac{R_o + R_i}{2}\mu_{friction}F \tag{16}$$

Put (4) into (1) and rearrange with (3),

$$\omega\frac{R_o + R_i}{2}\mu_{friction}F = \mu N^2 \frac{{R_o}^4 - {R_i}^4}{C_{Th}} \tag{17}$$

$$\omega = \frac{2\pi N}{60} \tag{18}$$

$$\frac{R_o + R_i}{2}\mu_{friction}F = \mu N \frac{{R_o}^4 - {R_i}^4}{C_{Th}}\frac{30}{\pi} \tag{19}$$

$$C_{Th} = \frac{60}{\pi}\frac{\mu({R_o}^2 - {R_i}^2)(R_o + R_i)N}{\mu_{friction}F} \tag{20}$$

Therefore, if the friction coefficient and dynamic viscosity is known, the gap of Air film C_{Th} can be represented by a function of rotational speed (N) and applied load (F).

Table 4-1 Various parameters in test condition [21]

Dynamic Viscosity(μ) of Air at Room Temperature (23°C)	$2.1808 \times 10^{-5}\ kg/m \cdot s$
Friction Coefficient($\mu_{friction}$) between Mole and Stainless steel	≈0.19
Outer Diameter of Top Foil(R_o)	$0.154m$
Inner Diameter of Top Foil(R_i)	$0.081m$

By substituting fixed values and rearranged, the Bearing Clearance (C_{Th}) can be represented by the function of RPM and the applied load.

$$C_{Th\approx} \approx 8.837 \times 10^{-6} \frac{N}{F}(m) \tag{21}$$

Chapter 5

Experimental Setup

5.1 Manufacturing of Hydrostatic Thrust Air Foil Bearing

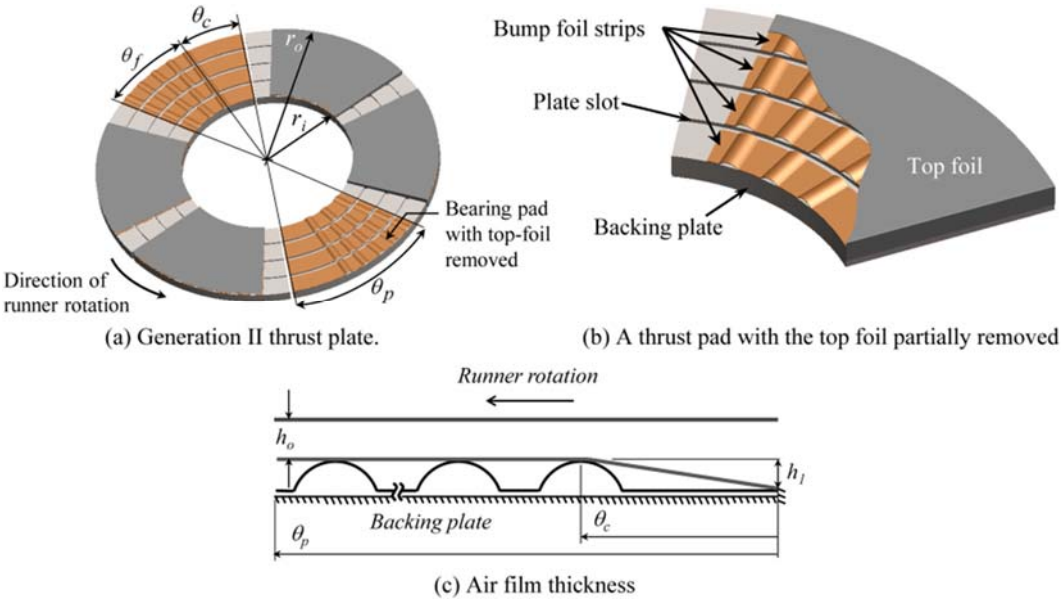

(a) Generation II thrust plate.

(b) A thrust pad with the top foil partially removed

(c) Air film thickness

Figure 5-1 Components of the bump foil bearings

The thrust air foil bearing is composed of four parts: top foil, bump foil, back plate and orifice holders. Each component of the thrust air foil bearing performs an important role to decide a characteristic of the foil bearing system. The top foil is supported by bump foil strips, and it carries a distributed load to the bump foil layer found underneath. Top foil is nothing different with bearing surface, so it is coated with lubricants to decrease the start-stop friction. The Corrugated bump foil acts as a spring, and it gives compliance to the bearing. So, the shape and material of the bump foil is an important factor in deciding bearing properties. The back plate is fixed with test rig as well as the supports foil bearing system. 32 holes around the back plate supply distributed air pressure. Orifice holders not only holds tongs from the top foil but also make all the

foils parallel with thrust runner. Therefore, a significant amount of time for the setting experiment test rig is required in air foil fabrication.

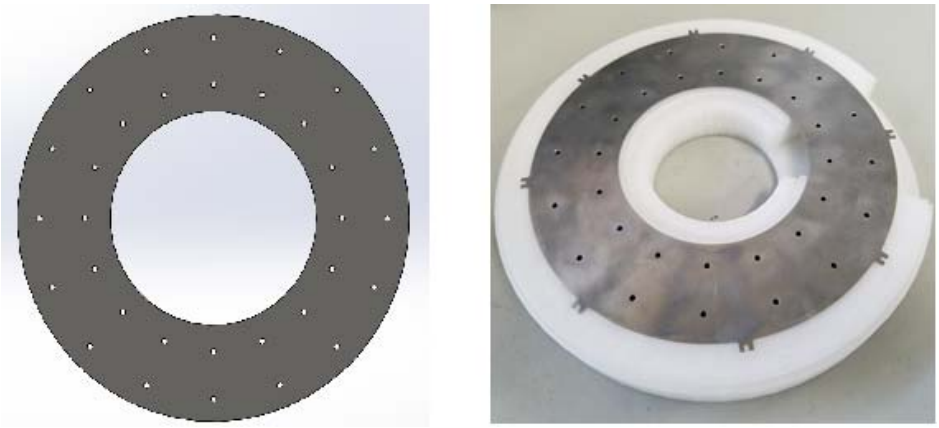

Figure 5-2 Solid model and Photo of the Top Foil

The fabrication processes of the top foil commence from the EDM cutting process (Electronic Discharging Machining). Unlike the radial bearing, the top foil of the thrust air foil bearing should be flat to be parallel with the thrust runner. As a result, the material of the top foil is made of stainless steel for convenience. Once the top foil is shaped, extrude parts (orange circle) are needed to be attached to the holes of the top plate. Because the contact surface is very thin (0.2mm) it is required to adhere together, laser welding is recommended for this process.

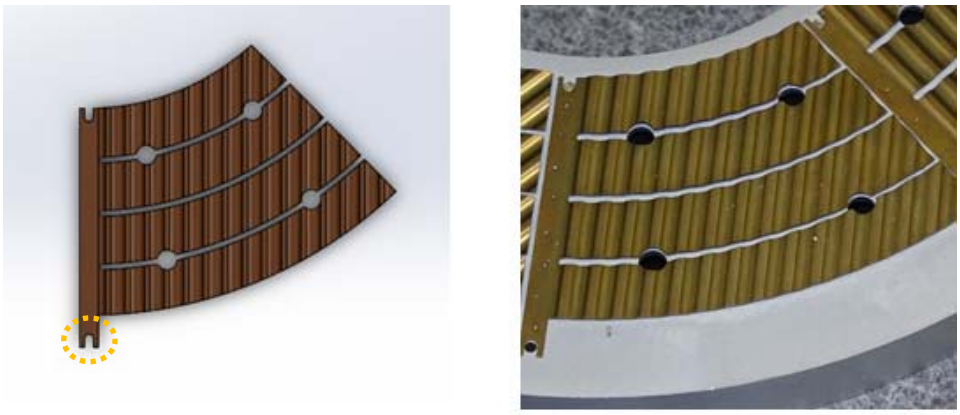

Figure 5-3 Solid model and Photo of the Bump Foil

The fabrication process of the bump foil proceeds as follows:

1. Blanks are cut out from a foil sheet for suitable size.
2. The blanks are supported on the jigs for forming bump shapes and pressed using a hydraulic press.
3. The formed bumps are then heat treated suitably.
4. Finally, EDM process is carried out for cutting the formed foils to the correct profiles.

Figure 5-4 Solid Model and Photo of the Back Plate

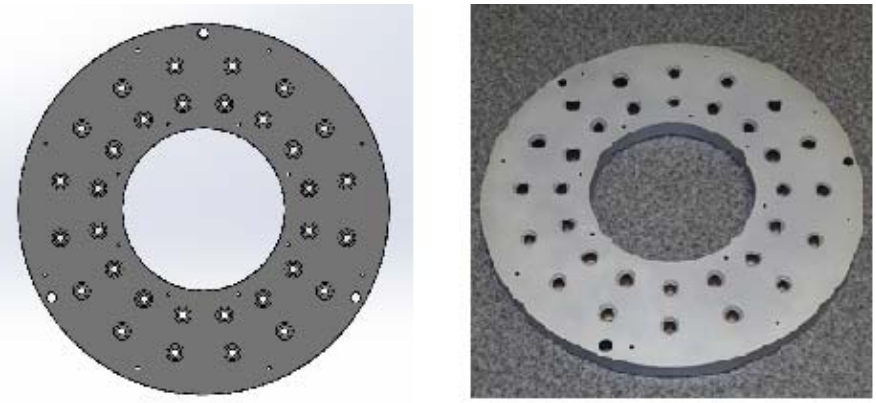

The back plate acts as a motherboard of a computer system because it contains all the critical components of the foil bearing. For this reason, the back plate is designed to be sturdy not only structurally but also thermally. Even though the back plate does not create friction with the runner, a covered surface is required. This is due to the difficulty of removing rust and dust once the bearing is assembled, cleanliness and corrosion resistance is very important to the back plate. Preventing corrosion, abrasive blasting is processed to the required surface condition. Further, the plate was electroplated to improve corrosion resistance.

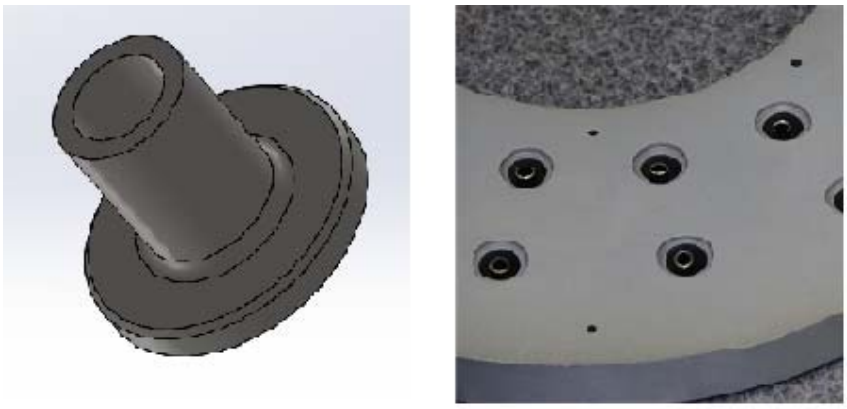

Figure 5-5 Solid Model and Photo of the Orifice Holder

There are 32 orifice holders located on the back plate containing 32 tongs from the top foil. Preventing local stress in the foil system, all the holders are manufactured in the same shape and size. The tongs from the top foil and the orifice holders will fit exactly, and the back plate and the orifice holders will have a loose fit.

(A) (B)

Figure 5-7 Bump Foils are fixed with Back Plate after Spot Welding

(A) Top View (B) Side View

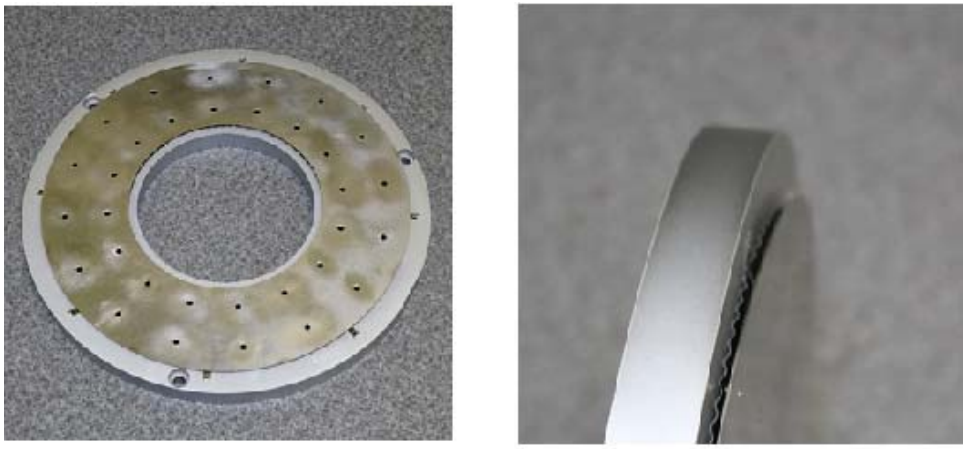

(A) (B)

Figure 5-6 Building up the Thrust Air Foil Bearing Assembly

(A) Top View (B) Side View

Once all the components are manufactured, they need to be put together to make a foil bearing assembly. The assembly processes of the bump foil are as follows: Fix the bump foils and plate in place and secure with masking tape. Next, perform spot welding of the bump foils to the plate. Next, place the top foils onto the bump foils. Finally, connect orifice holders to the top foil explains building process for the thrust air foil bearing assembly process.

Still, local stress will remain after assembling, due to a tolerance error in all the components, which causes for the top foil to be easily bent. Local deflection is a result of the bend creating degradation regarding load carrying capacity. To prevent the degradation, attach the high number sandpaper on the flat precision table, and do a grinding process as follows. Figure 5-8 explains the process in detail.

(A)

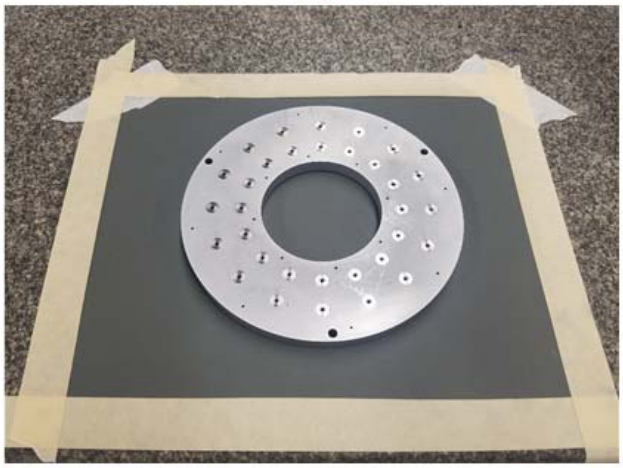

(B)

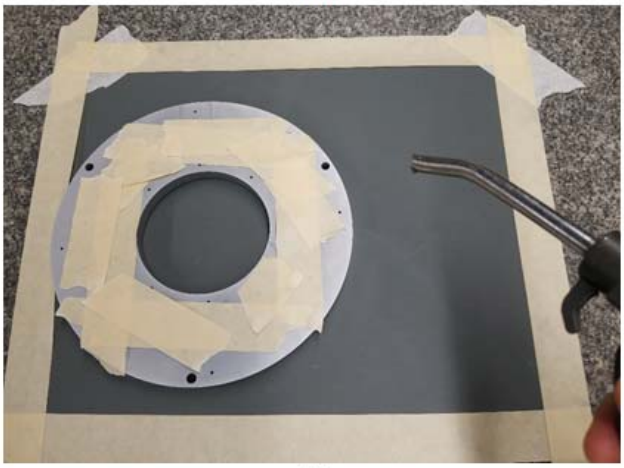

(C)

Figure 5-8 Grinding Process of the Foil Assembly

(A)Put a fine sand paper on the granite plate.

(B)Put on the bearing on the sand paper without any dust.

C)Seal up all the holes on the top and move the bearing cautiously. Make be moved like in a figure 8 and 90° turn every min to make a flat surface. Continue process for 20 minutes. When finished, clean each bearing hole with the air and vacuum gun.

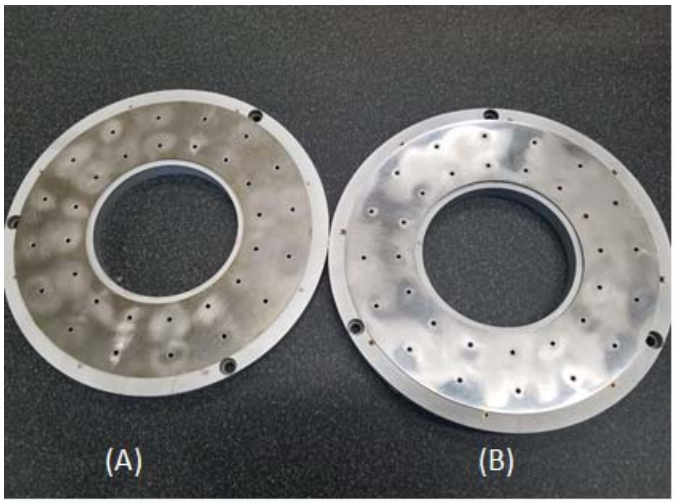

Figure 5-9 Comparison of Before and After Coating Process

(A)Before Coating (B) After Coating

5.2 Coating Process of Hydrostatic Thrust Air Foil Bearing

The coating process is an important procedure that improves bearing performance. Molybdenum disulfide (MoS_2) is a chemical which is widely used as a solid lubricant like graphite. Unlike the graphite, it is barely affected with absorbed vapors or moisture, and has a stable and low coefficient under experiment conditions. The following table shows the characteristics of typical Molybdenum disulfide coating.

Table 5-1 Specification of the Typical Molybdenum Disulfide Coating [29]

Load Capacity (ASTM 2625B)	1720 MPa
Wear Life (ASTM 2625A)	250 min.
Salt Spray Resistance (ASTM B117)	500 hrs.
Coefficient of Friction (ASTM D1894)	0.19 static / .16 kinetic
Abrasion resistance (mil STD 141A)	10,000 RPM

Thickness	.001” -.003” (0.0254 to 0.0762 mm)
Use Temperature	200°C

After assembling, the air foil thrust bearing is coated by Molybdenum disulfide and must be kept out of sunlight and wind for a couple of days. Figure 5-10 shows the picture of coated air foil thrust bearing.

Figure 5-10 Molybdnum Desulfide Coating on the Thrust Air Foil Bearing

5.3 Tension bolt tools

In the bearing experiment, runner and rotating shaft should be moved like a single body even in high speed. Meeting this requirement, both parts are connected very tightly. The Tension control bolting system has quickly become the most widely used method of tensioning high strength structural bolts. The ease of use and economic benefits has provided tens of thousands of projects with consistent, reliable, and economical steel connections. By referring the

commercial design, optimized tension tool by operating the pneumatic system for the test rig is designed. Figure 5-12 and Figure 5-11 show the solid model and manufactured tension tool.

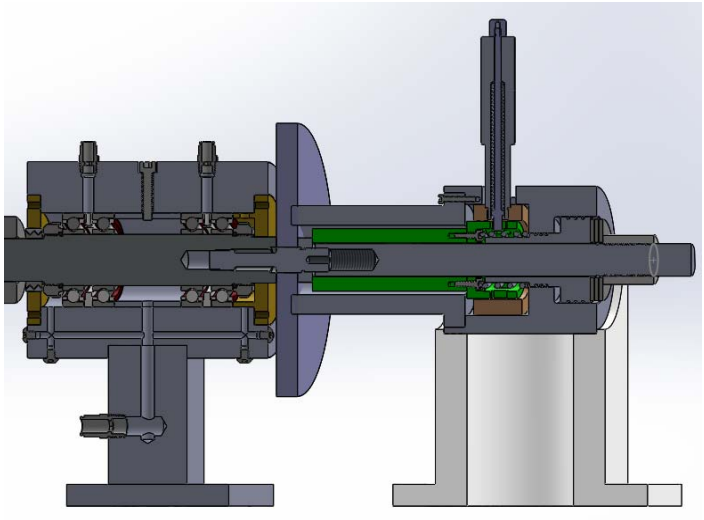

Figure 5-12 Solidmodel of Tension Tool

Figure 5-11 Photo of Tension Tool

5.4 Test Rig Setup

This chapter explains how to set the test housing. The main purpose of the test housing is supporting the shaft and air foil system as well as transmitting power from the electronic motor.

The test rig is composed of mainly four parts: hydraulic actuator, bearing support, runner support and 3kW electronic motor.

Also, use a load cell to measure torque and load, pressure gauge, proximity sensor for measuring the distance between the bearing plate and runner, five thermocouples for sensing five different positions from the back plate. Figure 5-12, 13, 14 shows the configuration of the test rig assembly and the Table explains each component's role in the test rig.

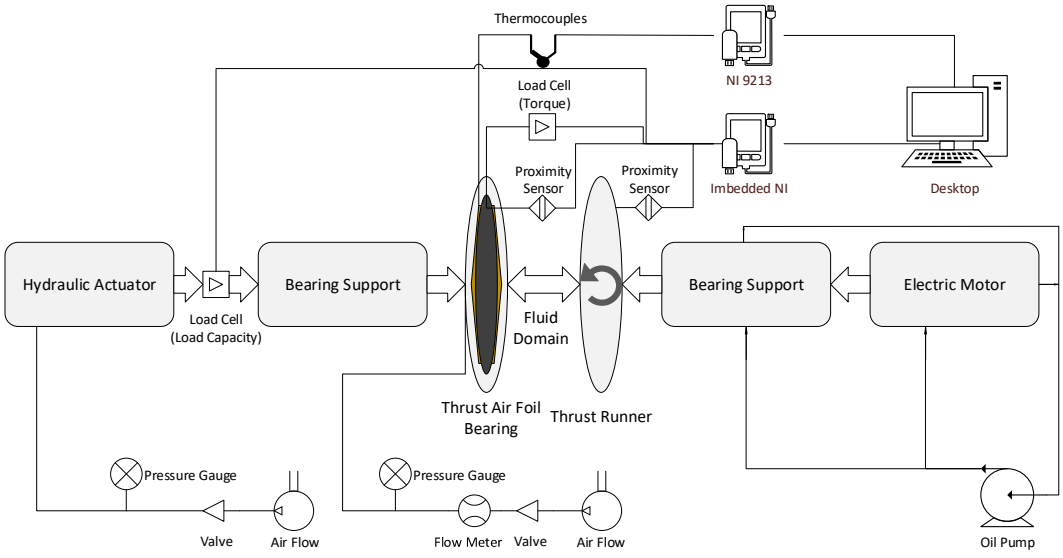

Figure 5-13 Schematic View of the Thrust Air Foil Bearing Test Rig

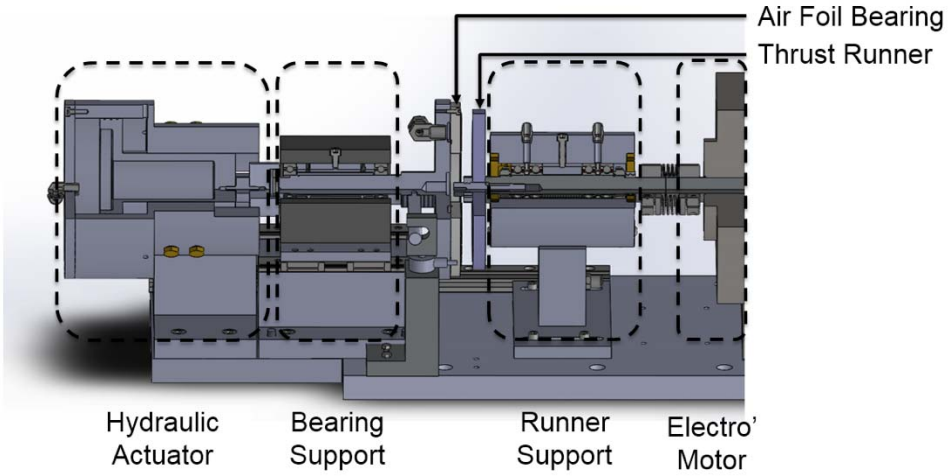

Figure 5-14 Solidmodel Design of the Thrust Air Foil Test Rig

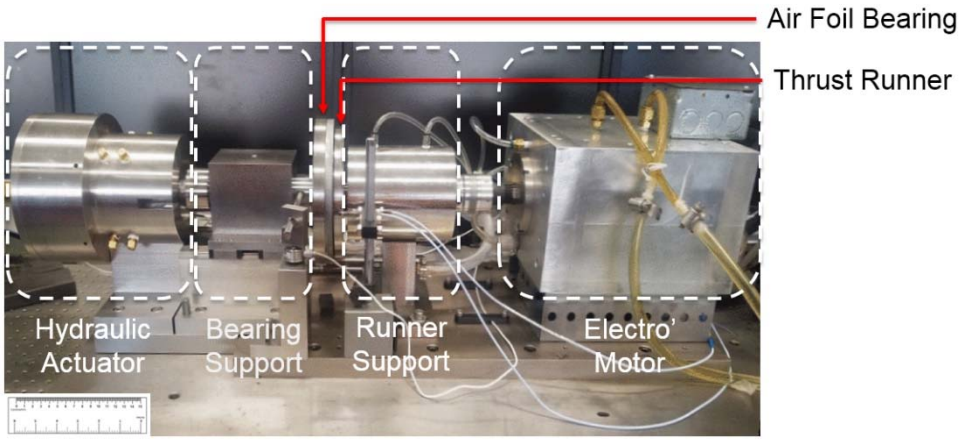

Figure 5-15 Photo of the Thrust Air Foil Test Rig

Table 5-2 Description of Each Component of the Test Rig

Components	Description
Hydraulic Actuator	Operated by supplied air. Apply load on the foil bearing system.
Bearing Support	Support air foil bearings. Transmit load from the hydraulic actuator.
Runner Support	Support thrust runner. Transmit power from the electronic motor Absorbs vibration from the electronic motor
Electro Motor	Up to 30000rpm. 3kW, Custom-made.

5.5 Sensor Instrumentation

After setting up the test rig, a measuring parameter is needed to understand the characteristic of bearing motions. The following parameters are: temperature, pressure, torque, and axial load. In this chapter, description of the torque, load, pressure, displacement, and temperature is loaded. After that, the explanation of the calibration will be attached. The detailed specification of the sensors is shown below. (Table 5-3)

Table 5-3 Description of the Calibration System

Measuring Parameter	Sensor	Brand Name, Company	Quantity
Axial Load	Load Cell	WMC-500, Omega	1
Friction Torque	Load Cell	WMC -50, Omega	1
Back Plate Pressure	Pressure Transducers	PX-409-100, Omega	1
Displacement	Proximity Probe	Bently Nevada, GE	2

Bearing Temperature	K -Thermocouples	K-type, Omega	5

Load carrying capacity is the most vital parameter, which affects the bearing's performance. Load capacity can be determined from applying load when the friction torque increases rapidly. Therefore, two load cells are installed for measuring applied load and friction torque respectively. In the experiment, load cells from OMEGA wmc-500 and wmc-50 are used.

From a distance data between runner and bearing, we can measure the stiffness which is another parameter that affects the performance of the bearing. It can be measured by the difference in distance measured by two proximity probes from their starting position.

Unlike hydrodynamic air foil bearings, the hydrostatic system controls the load capacity by changing the pressure within the air film. Pressure gauge at OMEGA can measure up to 100psi is installed at the end closest to the back plate. Also, pressure indicator with front panel connects with a pressure sensor for the calibration. Pressure data from the sensor will be used to figure out pressure profile along the foil bearing. A simple calculation is shown in Chapter 4, but in the experiment, it is not used because the calculation is suitable for the simple flat bearing case.

In various speed and load conditions, to figure out the temperature profile is very important key parameter because both rotational speed and axial load are responsible for heat generation with speed playing a more significant role in the magnitude of the temperatures. Type-K thermocouple sensors collect the temperature profile, and they are arranged in the multiple positions at the back plate. (See Figure 5-16)

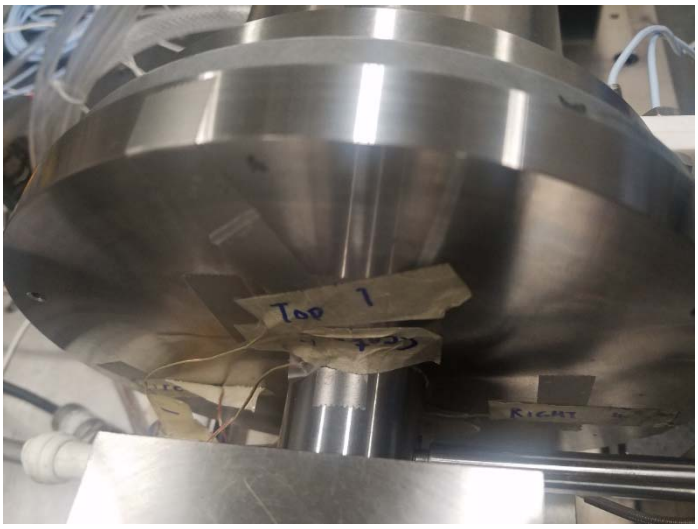

Figure 5-16 Thermocouples Installation at the Back late

5.6 Calibration

To measure the proper data from the sensors, eliminating sensor errors is required before doing the experiment. The Calibration defines the accuracy and quality of measurements recorded using a piece of equipment. The two error mechanisms common to all sensors are offset and gain error.

Offset error is the deviation from the minimum voltage expected when the minimum input is applied. Gain error is the deviation in the inverse slope of the transfer function, when the offset error is removed, from the ideal. For instance, a pressure gauge (input voltage) may be required to start from 0V to 100V (front panel may show 0 to 100psi), the actual transfer function (output voltage) may start from 5mV and finish at 35mV. In this case, the offset error is 5mV, and the gain error is 3000 (or 3 psi/V) The relationship can be described by the formula (22), is shown actual calibration process.

$$y = \frac{1}{g}x + o \tag{22}$$

$$y = output\ voltage\ , x = input\ voltage$$
$$g : gain\ error, o : output\ error$$

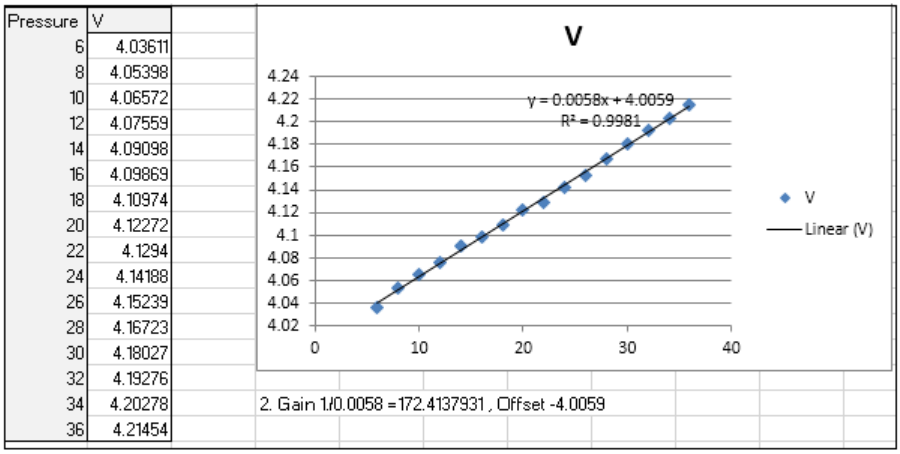

Figure 5-17 Pressure sensor calibration

The above figure is the graph of the pressure sensor calibration. Likewise, load cells and proximity probes are also adjusted before measurement. After that, Data acquisition is processed by using LABVIEW program.

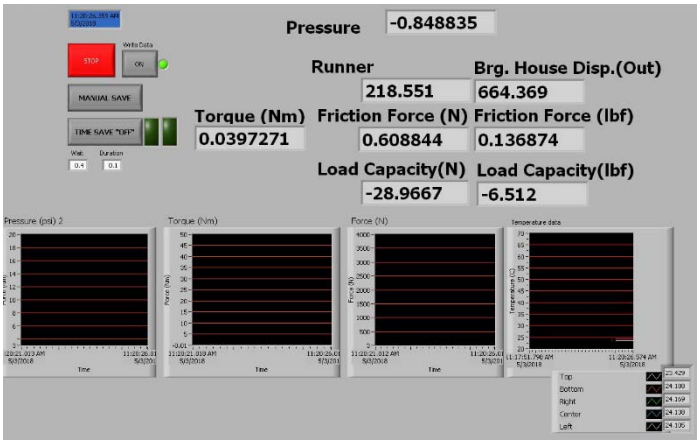

Figure 5-18 LABVIEW front panel

Chapter 6

Experimental Result

6.1 Test Result (Thrust Air Foil Bearing)

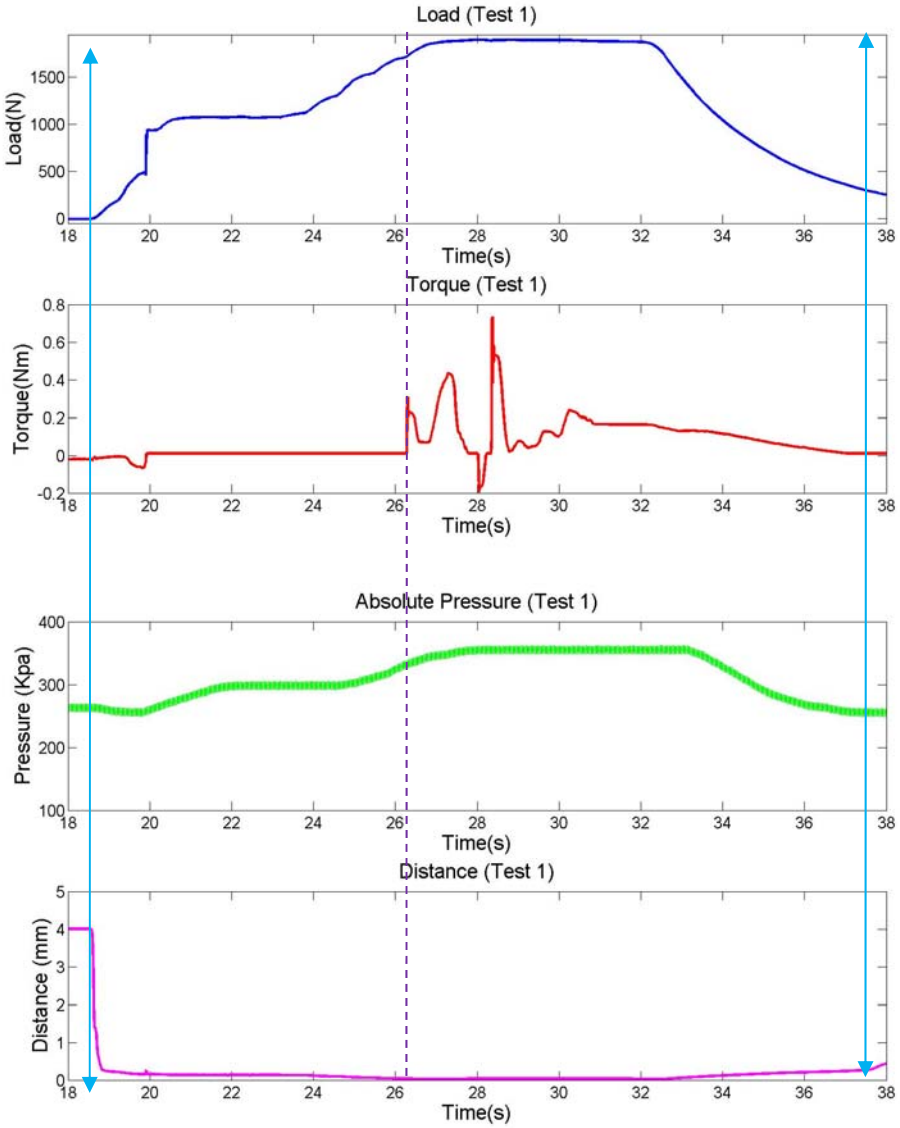

Figure 6-1 Test 1 Result

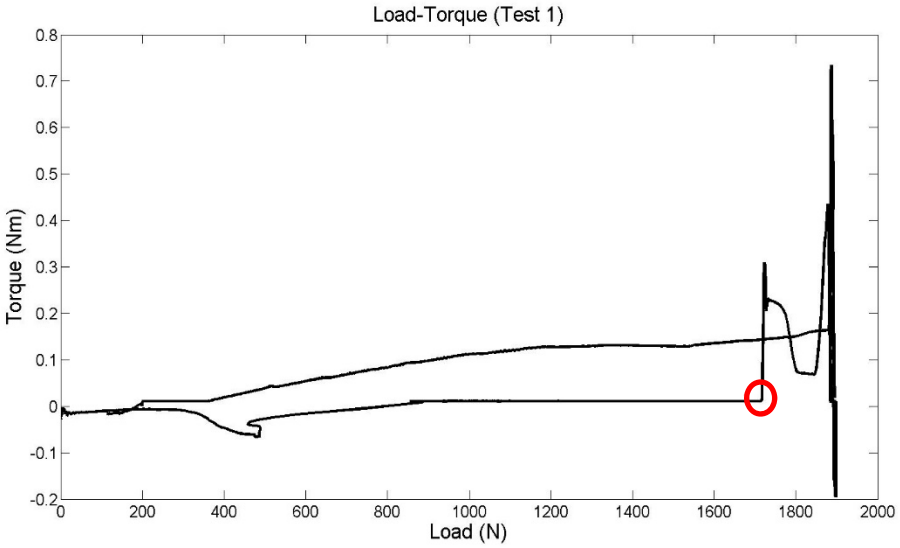

Figure 6-2 Load-Torque Plot for the Test 1

Table 6-1 Test 1 Result

Test	1
Contact Time	19s to 37s
Pressure Change	250kpa to 350kpa
Load Capacity	1720N

Figure 6-1 and Figure 6-2 shows the test1 result. The blue arrow lines are shown contact time between thrust and runner, and it does mean the bearing system is working at the time (from 19s to 37s). During the time, the pressure also arises, because the air film also be pressurized by the apply load (from 250kpa to 350kpa). The purple dotted line shows the friction torque occurs between runner and bearing, and The apply load at that time denotes load carrying capacity; the bearing system can operate safely under load capacity (1720N). According to the test result, The bearing system can support thrust load up to 1720N, and it is almost three times higher than a flat bearing system (pocket and recess thrust air foil beairng) with the same size. Different tests are attached as follows.

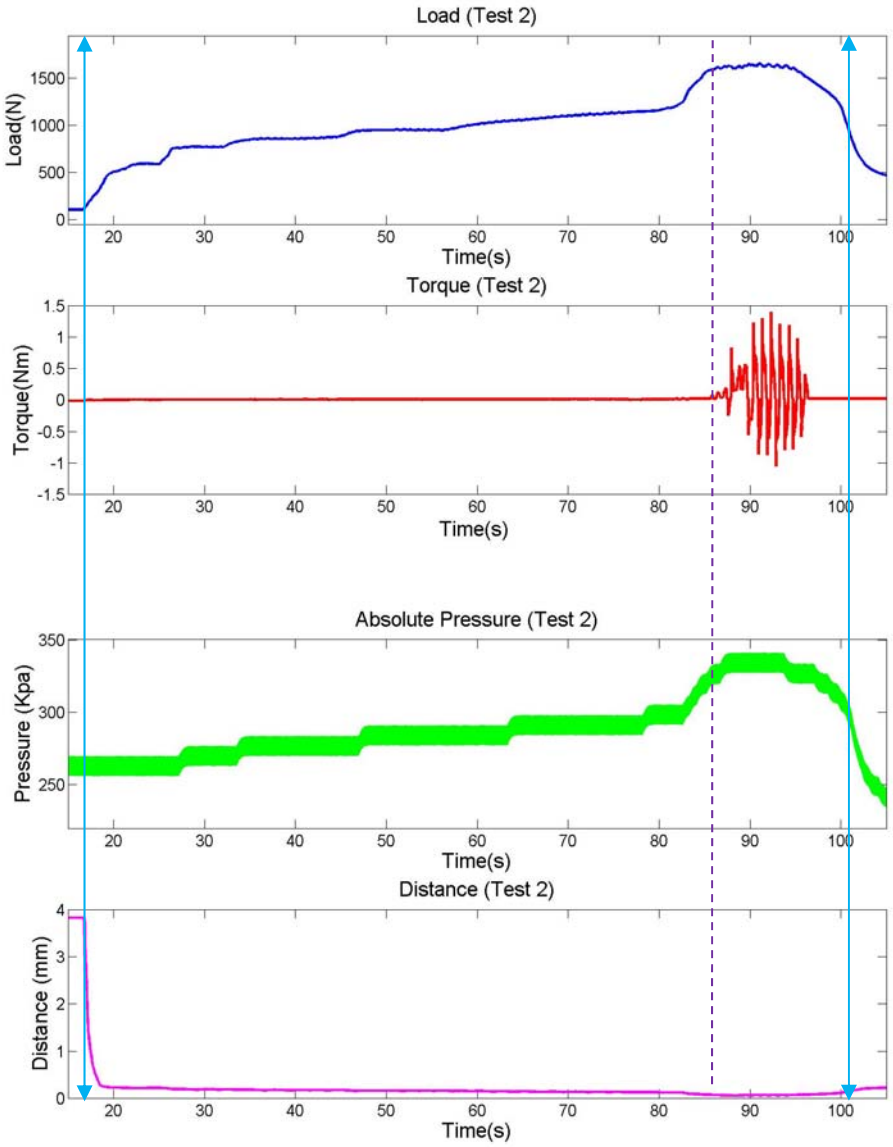

Figure 6-3 Test 2 Result

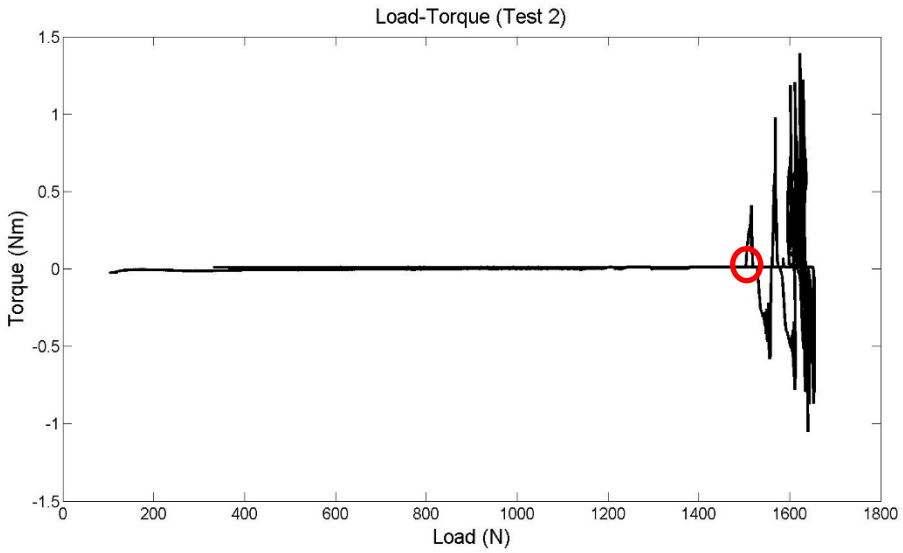

Figure 6-4 Load-Torque Plot for the Test 2

Table 6-2 Test 2 Result

Test	2
Conatact Time	17s to 100s
Pressure Change	250kpa to 330kpa
Load Capacity	1520N

Test 2 shows lower load carrying capacity compared with Test 1. After the Test 1, Alignment process between the bearing and the runner is performed to achieve higher load capacity. Unfortunately, it does make more run out than before, and it leads to deterioration of load capacity. The result shows that the hydrostatic thrust air foil bearing system is very sensitive to parallel alignment.

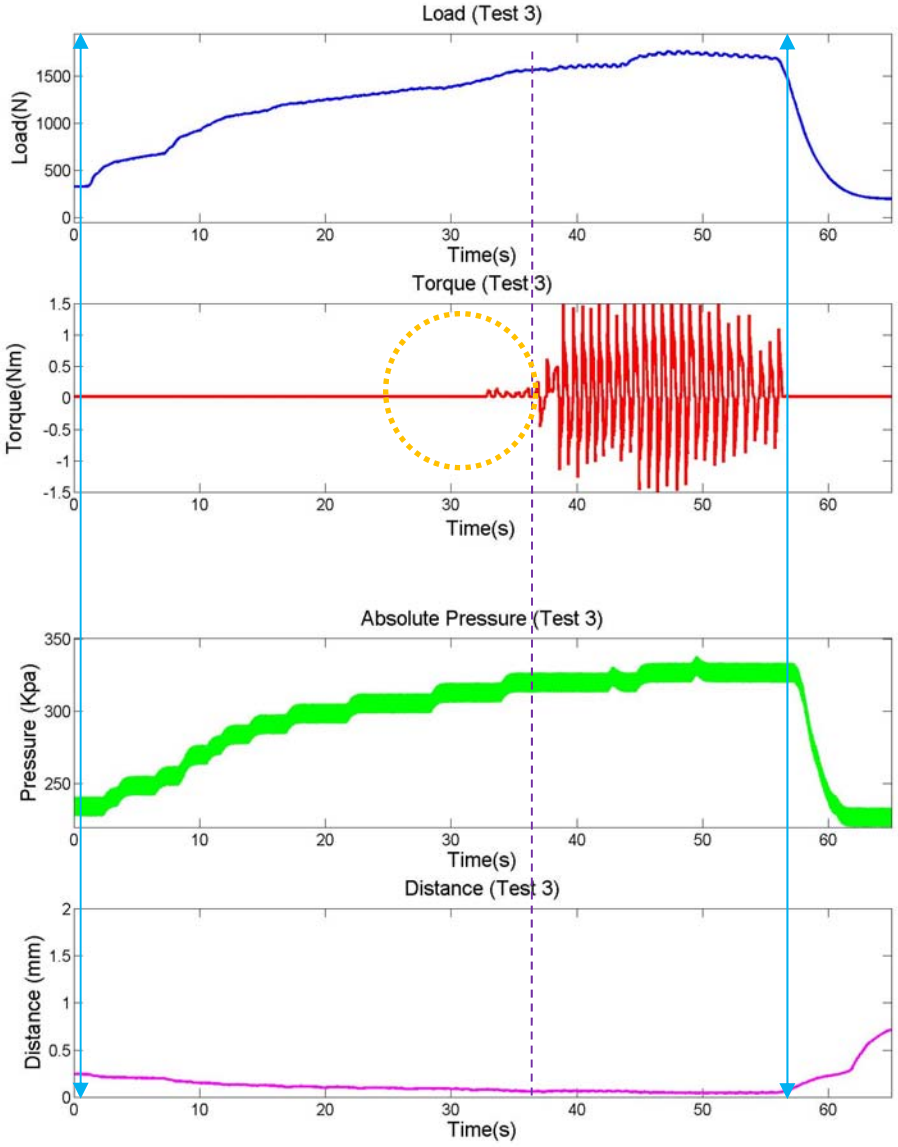

Figure 6-5 Test 3 Result

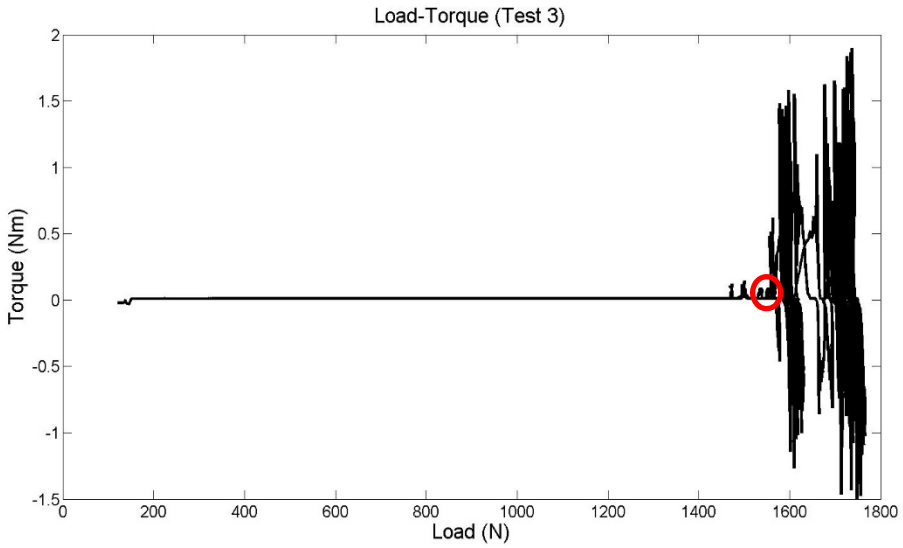

Figure 6-6 Load-Torque Plot for the Test 3

Table 6-3 Test 3 Result

Test	3
Conatact Time	1s to 60s
Pressure Change	230kpa to 300kpa
Load Capacity	1520N

Test 2 and test 3 are experimented in a series. Subtle changes of friction torque from 32s to 36s does not mean the bearing system reaches load capacity (orange circle in torque plot). It is just because applied load under load capacity makes ball bearing shaft move, and the torque sensor catches this movement. Friction torque for reaching load capacity is shown after 37s, and the load capacity of test 3 is same as test 2 result.

6.2 Test Result (Damaged Hydrostatic Thrust Air Foil Bearing)

If the bearing is loaded more than its load capacity, the bearing undergoes wear and subsequent damage. Overload causes contact friction between the bearing and runner, and it changes the top foil finish from polished surface to scratched rough surface. It also causes heat generation which makes wavy and twisted top foil. In this chapter, the test result with damaged thrust air foil bearing is shown (Figure 6-7), and the degradation from damage is explained.

(A) (B)

(C)

Figure 6-7 Photos of Damaged Hydrostatic Thrust Air Foil Bearing and Runner

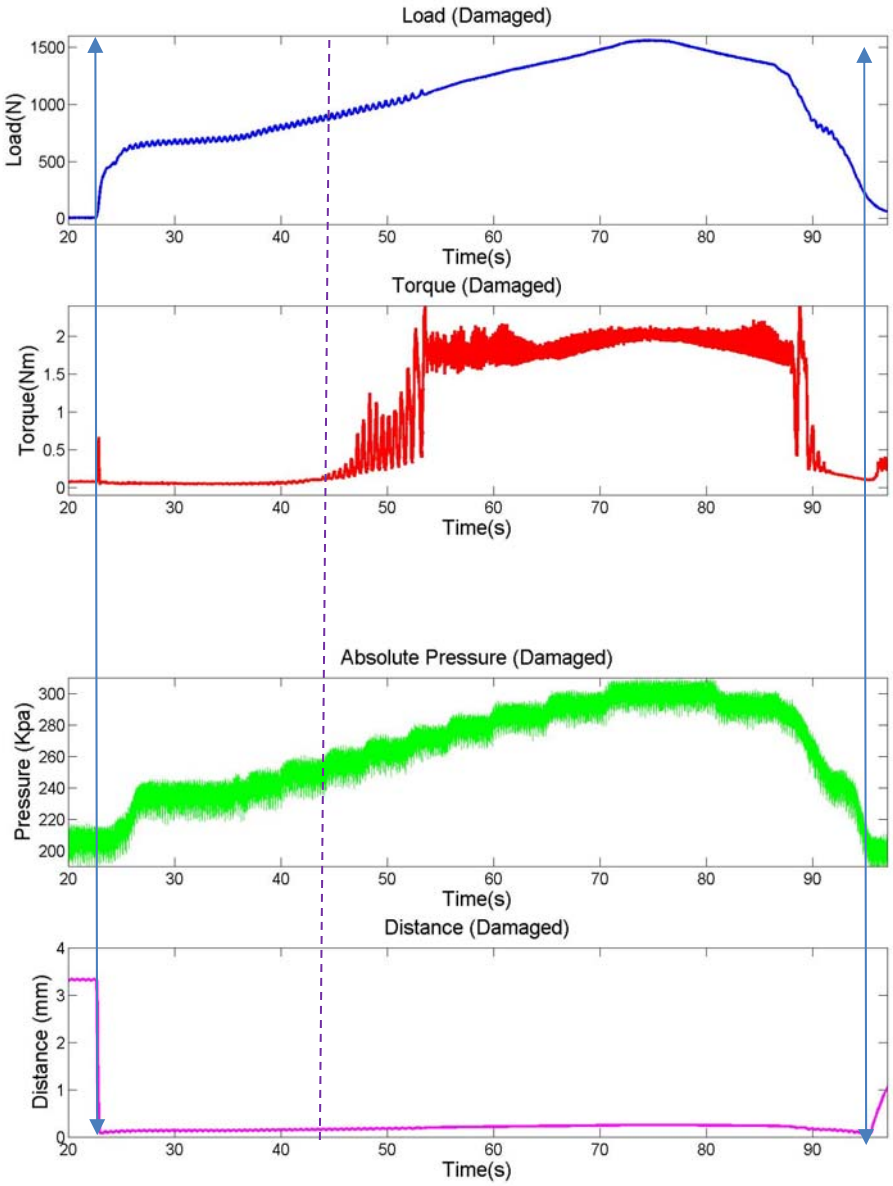

Figure 6-8 Damaged Hydrostatic Thrust Air Foil Bearing Test Result

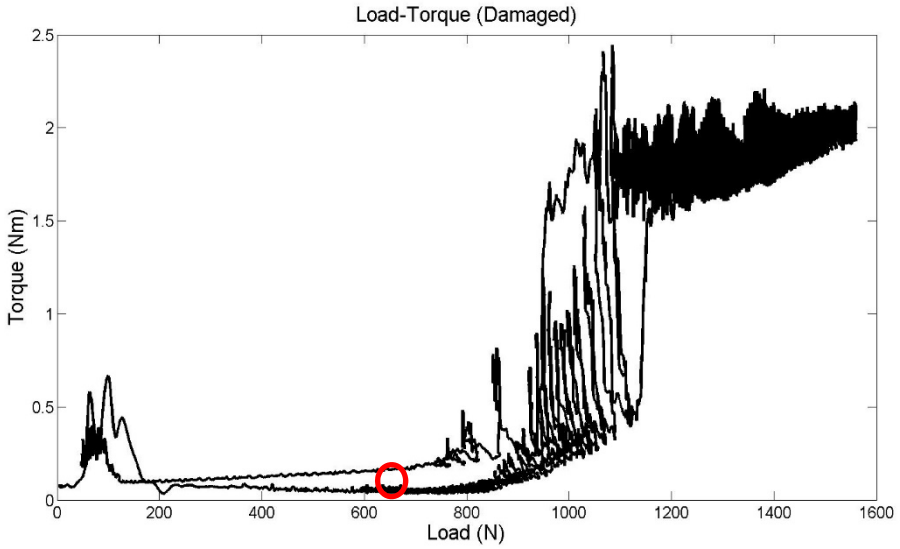

Figure 6-9 Load-Torque plot for the Damaged Hydrostatic Thrust Air Foil Bearing Test

Table 6-4 Damaged Hydrostatic Thrust Air Foil Bearing Test Result

Test	Damaged Air Foil Bearing Test
Conatact Time	22s to 95s
Pressure Change	210kpa to 300kpa
Load Capacity	800N

Figure 6-8 and Figure 6-9 shows the result of the Damaged Air Bearing Test. Compared to the test 1,2 and 3, load capacity is degraded more than 40%, because twisted top foil and the scratched surface cannot make an air film with high pressure. From the result, the operating bearing system under load capacity is very important to sustaining bearing performance.

6.3 Test Result (Hydrostatic Thrust Flat Air Bearing; Pocket / Recess)

Flat air bearings are one of the simplest type of the hydrostatic air bearings can make pressurized air film. However, the concept of bearing is developed long time before the invention of the air foil bearing, there is a vibration and noise issue called pneumatic hammer due to pneumatic instability, and it is mainly occurred in thrust bearings. The cause, for such instability, is the delay of dynamic pressure response within the recess cavity control volume which occurs due to compressibility effects [30] [31]. The pneumatic hammer issue can be avoided to make the air film as a damper.

In respects of design, the back plate, bearing without the foil system, can function as a flat air bearing. The back plate is manufactured with counterbore holes which enables us to test in two different ways (Recess air bearing, Pocket air bearing).

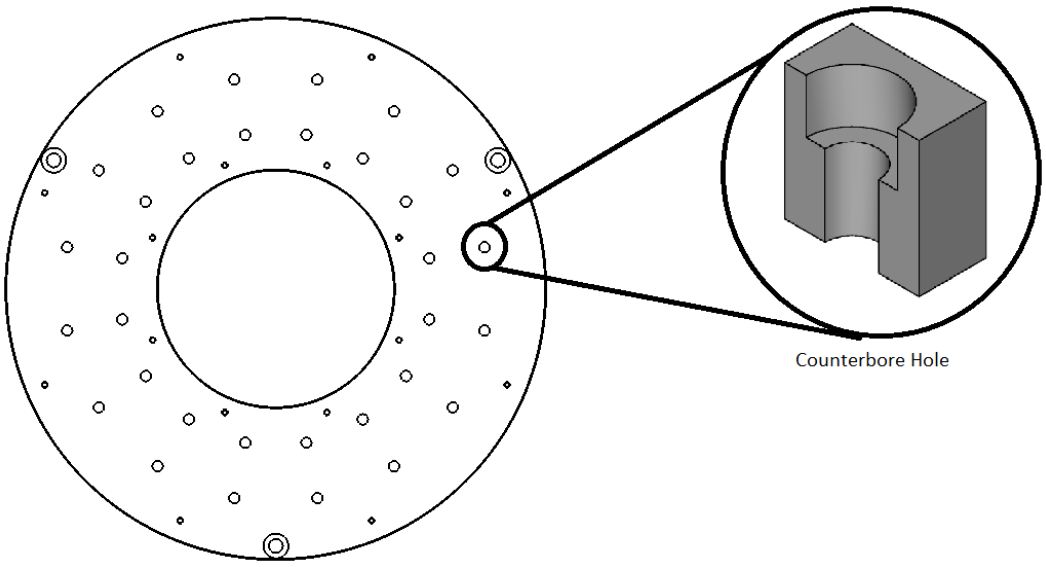

Figure 6-10 Back Plate Can be used as a Thrust Flat Air Bearing

In this chapter, the results of the flat air bearing are listed and commented compare with the hydrostatic thrust air foil bearing results.

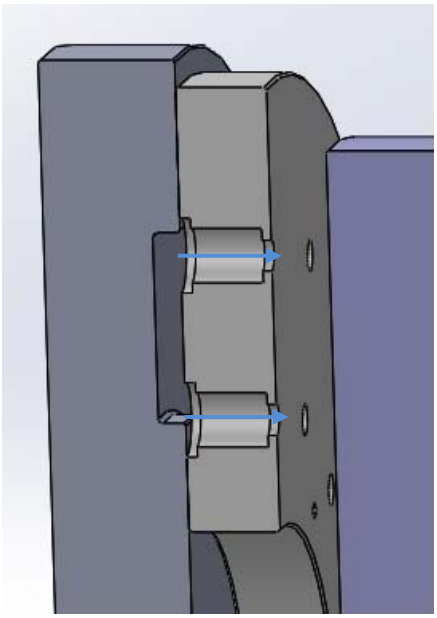

(A)

(B)

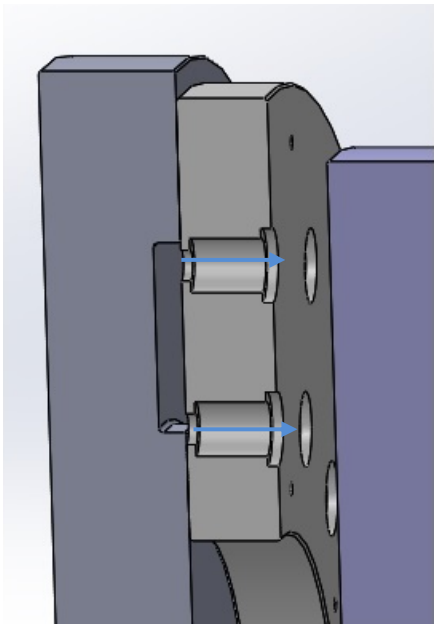

(C)

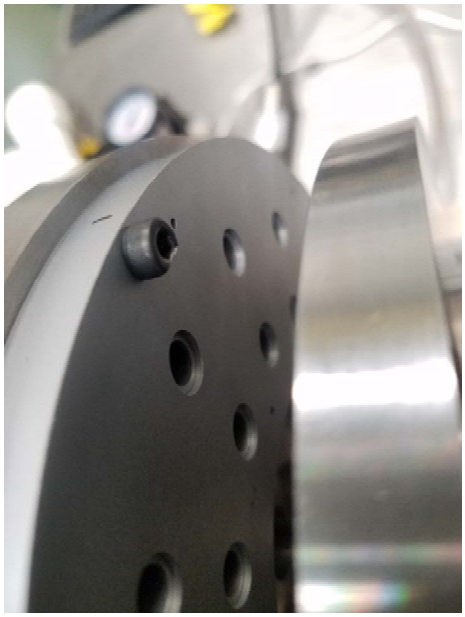

(D)

Figure 6-11 Soildmodel and Photo of Thrust Flat Air Bearing

(A),(B)- Pocket Air Bearing

(C),(D)- Recess Air Bearing

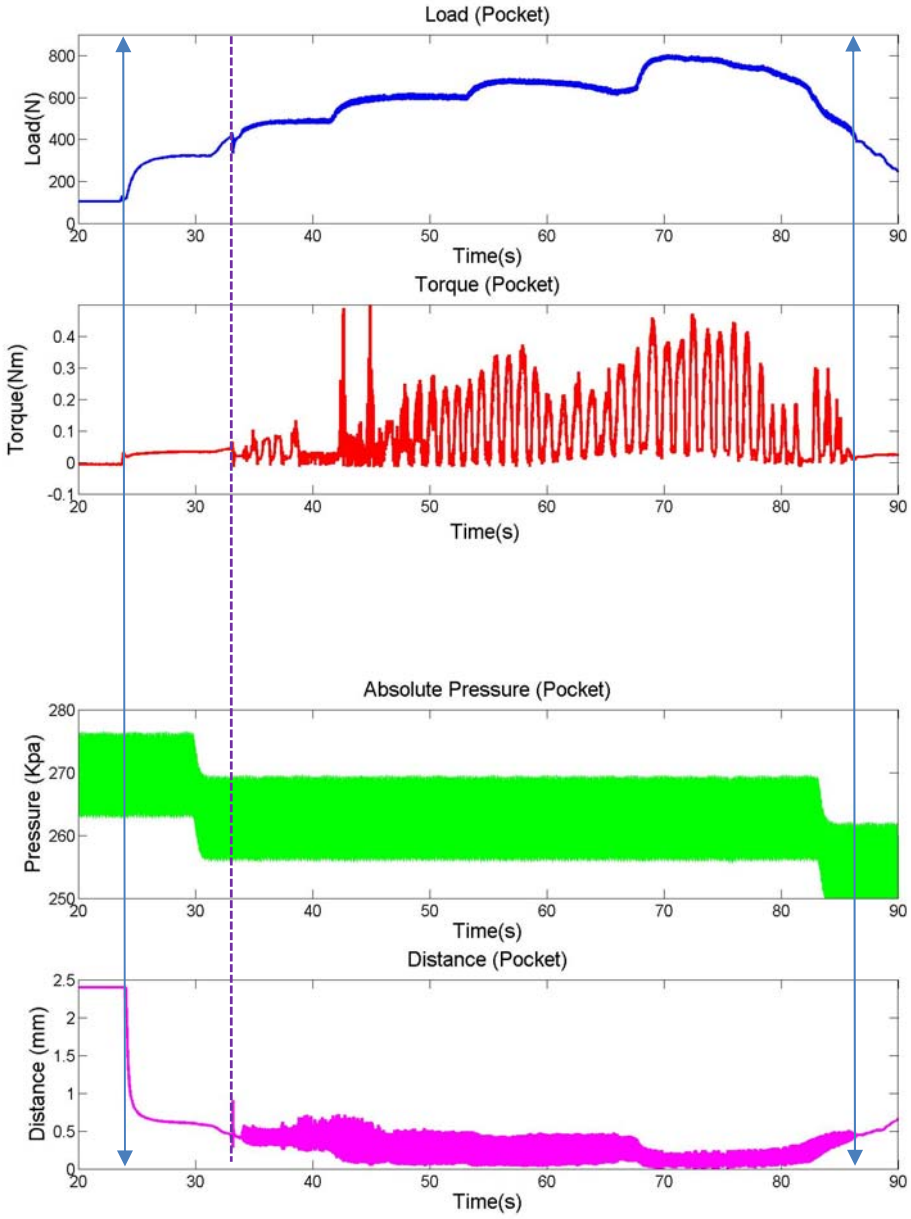

Figure 6-12 Pocket Flat Air Bearing Test Result

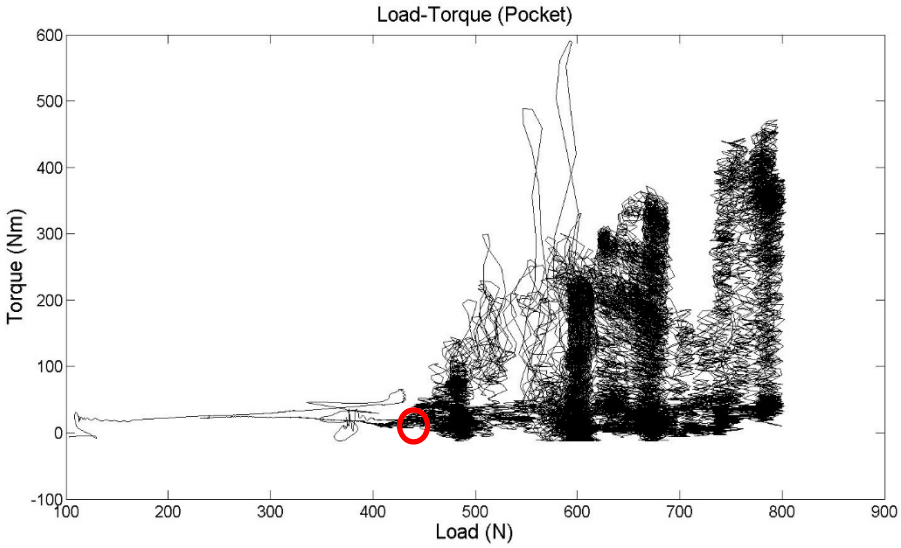

Figure 6-13 Load-Torque Plot for the Pocket Flat Air Bearing

Table 6-5 Pocket Flat Air Bearing Test Result

Test	Pocket Air Foil Bearing
Conatact Time	23s to 87s
Pressure Change	No change
Load Capacity	400N

As shown in Figure 6-12, Figure 6-13, and Table 6-5, the test of pocket bearing shows much lower load capacity(400N) compare to former results. During the experiments, the whole test rig has intensive shaking with a hammering noise near the load capacity (400N), and it is clearly shown in distance plot.

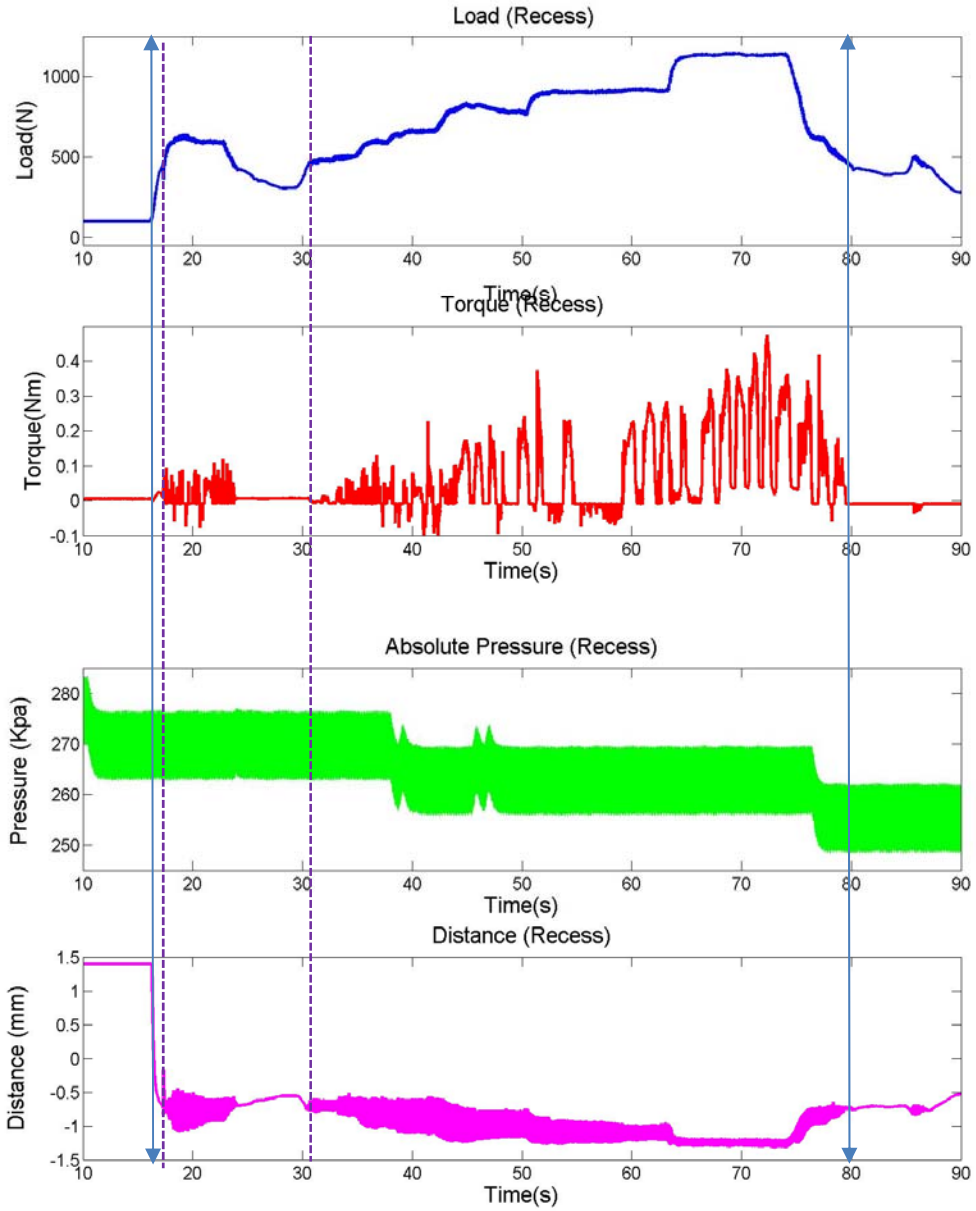

Figure 6-14 Recess Flat Air Bearing Test Result

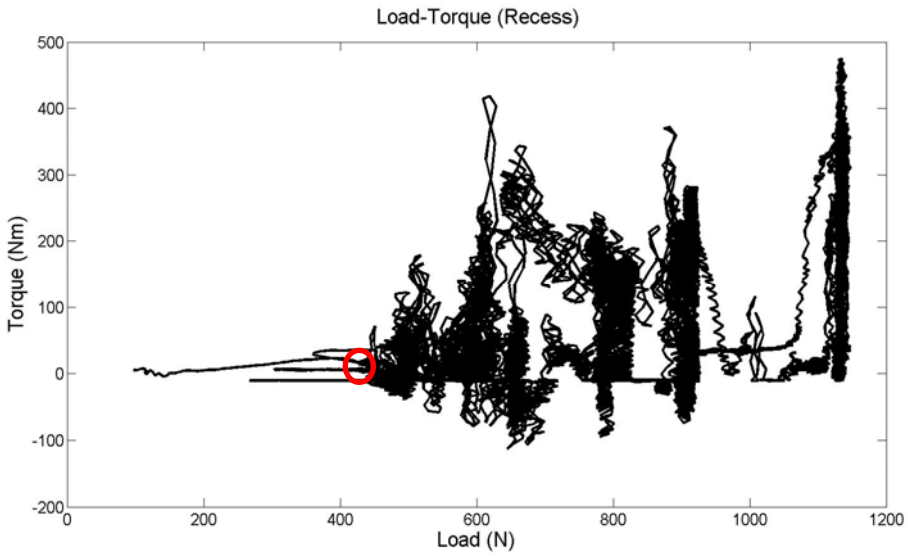

Figure 6-15 Load-Torque Plot for the Recess Flat Air Bearing

Table 6-6 Recess Flat Air Bearing Test Result

Test	Recess Air Foil Bearing
Conatact Time	13s to 80s
Pressure Change	No change
Load Capacity	420N

Figure 6-14, Figure 6-15 and Table 6-6 show test result of the recess air bearing. Likewise the pocket flat air bearing case, the whole test rig has intensive shaking with hammering noise near the load capacity (420N), and it is clealy shown in the distance plot.

Compare with the formal test, the load capacity of the both cases is 70% lower than the result of the thrust load carrying capacity, because the air film between the bearing and the runner does not work properly as a damper because of pneumatic hammer effect.

Even though the design of the bearing is different, the pneumatic hammering issue is occurred around in 400N. Throughout the study, both cases are not properly designed to avoid

hammering effect, and it mainly comes from the common big pockets positioned in the bearing support. As shown in Figure 6-16, the big pockets behind the back plate (orange circle) give pressure response delay(blue arrow) to the air film. The bearing and test rig themselves can resonate as the air film alternately compresses and expands(red arrow), and the resonation brings vibration and hammering noise.

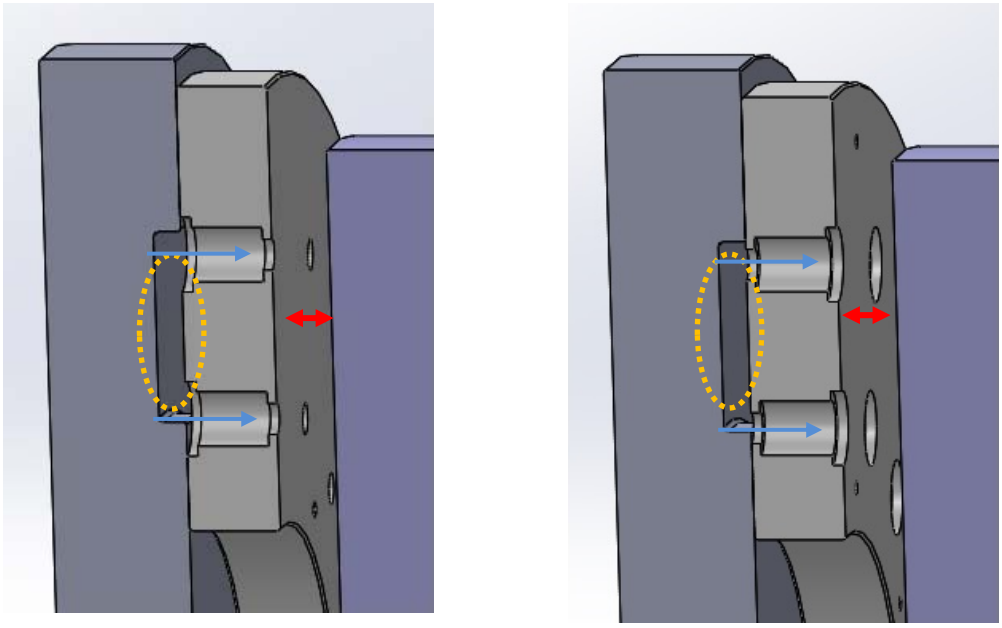

(A) (B)

Figure 6-16 The Process of Pneumatic Hammering Effect

6.4 Comparison with Theoretical Results

Based on the equation (12) in Chapter 4, the rough estimate of the load capacity can be calculated based on the flat air bearing with double grooves with same outer diameter (154mm). In addition, air film thickness can be calculated based on the load capacity and rotational speed. All experimental results are conducted on the low RPM speed, and Table 6-7 is shown the load capacity and film thickness of the each tests.

Table 6-7 Bearing Characteristics of the Experimental and Theoretical Results

	Type of Test	Load Capacity	Bearing Film Thickness (~50 RPM)
Experimental Results	Test 1	1720N	0.0026mm
	Test 2	1520N	0.0029mm
	Test 3	1520N	0.0029mm
	Damaged Foil Bearing	800N	0.0056mm
	Pocket Air Bearing	400N	0.0119mm
	Recessed Air Bearing	420N	0.0120mm
Theoretical Result	Flat Bearing with 2 Grooves	2086N	0.0021mm

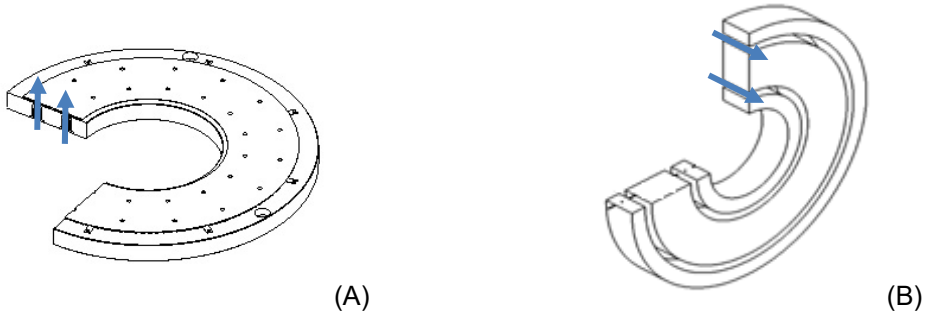

(A) (B)

Figure 6-17 Design Difference of the Test 1,2,3 and Theoretical Results

The load capacity from the theoretical result (2086N) shows much higher than experimental results, because the design of the theoretical flat air bearing (Table 6-7, (B)) has two circumferential grooves unlike the tested hydrostatic thrust air foil bearing (Table 6-7, (A)). In addition, the theoretical result is ideal case which is not assuming power loss such as misalignment issue.

The damaged bearing and flat bearing shows lower load capacity (800N) and thick air film (0.0056mm) compare to test 1,2 and 3 result. Scratched surfaces and twisted top foil do not function to make a thin air film with high pressure and it degrades the bearing performance.

The flat air foil bearing (pocket, recessed) has much lower load capacity (~400N) and thicker film thickness (~0.0120mm) compare with formal results, because vibration cannot maintain the pressurized thin film between bearing and the thrust runner. In other words, the thrust foil bearing makes a good damping structure between the bearing system, and it gives a good indication that hydrostatic thrust air foil bearing system gives enhanced load carrying capacity among the air bearing system.

6.5 Temperature Profile

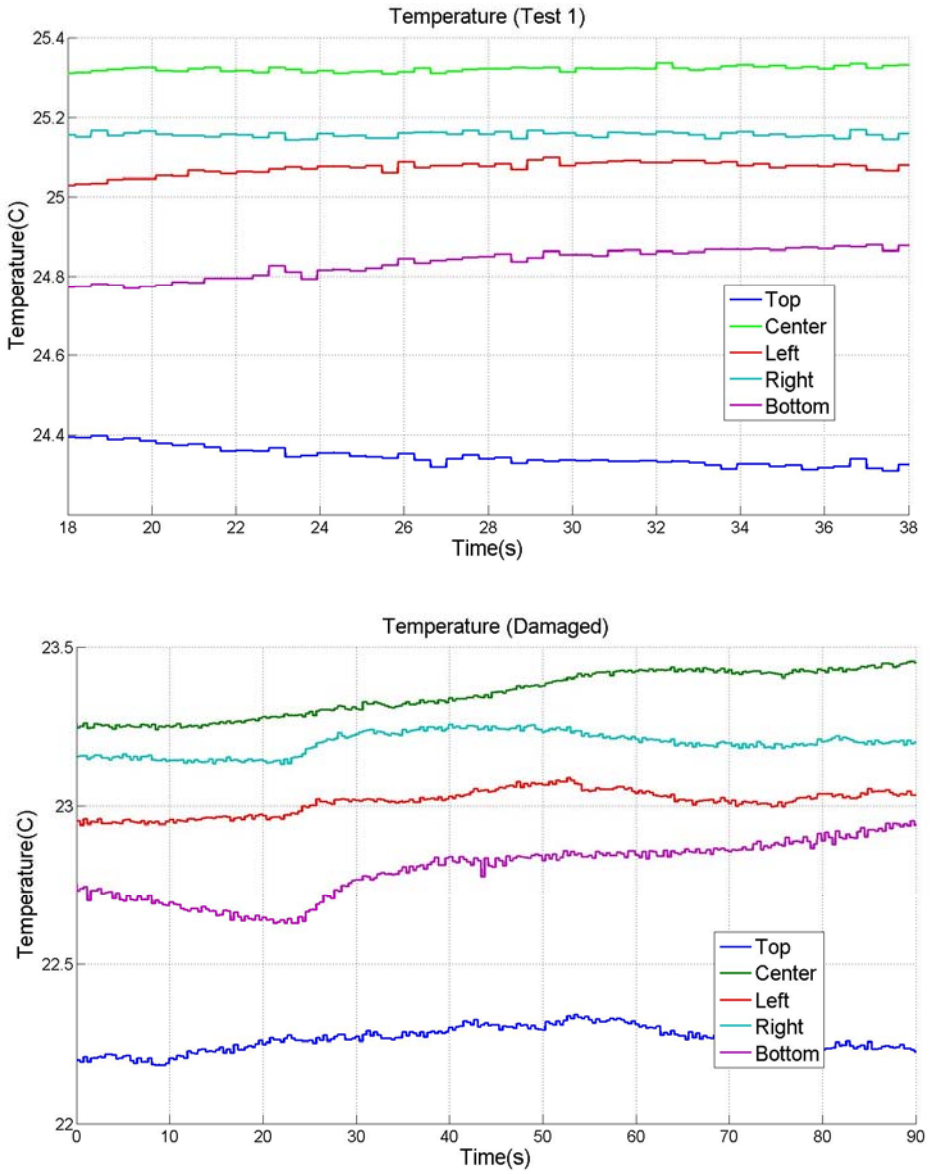

Figure 6-18 Temperature Plot of the Test 1 and Damaged Thrust Air Foil Bearing Test

Figure 6-18 shows temperature plot of the test 1 and damaged thrust air foil bearing test. During the test, the temperature does not change significantly over time, because test is

conducted in short time and low rotational speed (~50 RPM). In addition, the thickness of the back plate and bearing support is too thick to transfer the heat from the foil bearing. Knowing the heat generation from the bearing system, thermocouples should be positioned inside the thrust air foil structure.

Chapter 7

Conclusion

A hydrostatic thrust foil bearing was designed and experimentally tested. The load capacity was found to be 1.5kN. A simple analytical model was used to estimate the load capacity and the analytical model shows reasonable agreement with the experimental results.

The experiment revealed the high level of sensitivity of the load capacity to misalignment. The thrust foil bearing load capacity decreased significantly when there was minor misalignment of the thrust runner with the bearing.

The foils were removed and the bearing was operated as a rigid bearing. In the rigid bearing, significant pneumatic instability was observed. However, use of compliant thrust foil bearing mitigated pneumatic instability.

Finally, it is important to operate the bearing within its intended design limits. Operating the bearing beyond design conditions may result in degradation of bearing performance.

Chapter 8

Future Work

1. In this study, simplified analytical model is used to make a rough comparison with experimental result. Therefore, numerical solvers for modeling hydrostatic thrust foil bearings will be developed for exact validation.
2. One bearing is tested for the experiment, so after damage, the performance of the bearing is far more degraded than the formal test especially regarding the back plate pressure. Therefore, more bearings will be tested under damage safe region.
3. Module design arranges the test rig for testing a different kind of bearings. Therefore, improved and commercial thrust air foil bearings will be designed and tested. In addition, other characteristics such as stiffness and damping behavior will be analyzed in the following test.

References

[1] "Bearingindustry.com," Bearing Industry, [Online]. Available: http://www.bearingsindustry.com/Fluidfilmbearings.php.

[2] "Rolling Element Bearings," STI Vibration Monitoring Inc., 27 6 2017. [Online]. Available: http://www.stiweb.com/kb_results.asp?ID=53.

[3] R. H. Yadav, Development of Foil Bearing Test Rig, Arlington: The University of Texas at Arlington, 2013.

[4] "What is a hydrodynamic fluid film bearing?," Waukesha Bearings, [Online]. Available: https://www.waukbearing.com/en/technical-resources/faqs/?ID=2.

[5] Brian Dykas, Robert Bruckner, Christopher DellaCorte, Brian Edmonds, "Design, Fabrication, and Performance of Foil Gas Thrust Bearings for Microturbomachinery Applications," *Gas Turbines Power,* vol. 131, no. 1, 2008.

[6] G. L. Agrawal, FOIL AIR/GAS BEARING TECHNOLOGY ~ AN OVERVIEW, New York: American Society of Mechanical Engineers, 1997.

[7] Block, Van Rossum, The Foil Bearing- A New Departure in Hydrodynamic Lubrication, Lubrication Engineering, 1953.

[8] C. Dellacorte, M.J. Valco, "Load Capacity Estimation of Fil Air Journal Bearings for Oil-Free Turbomachinery Applications," vol. 43, no. 4, pp. 795-801, 2008.

[9] Daejong Kim, Jeongpil Ki, Youngcheol Kim, Kookyoung Ahn, "Extended Three-Dimensional Thermo-Hydrodynamic Model of Radial Foil Bearing: Case

Studies on Thermal Behaviors and Dynamic Characteristics in Gas Turbine Simulator," *Gas Turbines Power,* vol. 134, no. 5, 2012.

[10] Fangcheng Xu Daejong Kim, "Dynamic performance of foil bearings with a quadratic stiffness model," *Neurocomputing,* vol. 216, no. 5, pp. 666-671, 2016.

[11] Jason C. Wilkes, Jonathan Wade, Aaron Rimple, Jeff Moore, Erik Swanson, Joseph Grieco, Jerry Brady, "Impact of Bearing Clearnce on Measured Stiffness and Damping Coefficient and Thermal Performance of High-Stiffness Generation 3 Foil Journal Bearing," *Gas Turbines Power,* vol. 140, no. 7, 2018.

[12] Srikanth Honavara Prasad, Daejong Kim, "Scaling Laws for Radial Clearance and Support Structure Stiffness of Radial Foil Bearings," *Gas Turbines Power,* vol. 140, no. 7, 2016.

[13] Kyuho Sim, Jisu Park, "Performance Measurements of Gas Bearings With High Damping Structures of Polymer and Bump Foil Via Electric Motor Driving Tests and One Degree of Freedom Shaker Dynamic Loading TEsts," *Gas Turbines Power,* vol. 139, no. 9, 2017.

[14] Daejong Kim, An Sung Lee, Bum Seog Choi, "Evaluation of Foil Bearing Performance and Nonlinear Rotordynamics of 120 kW Oil-Free Gas Turbine Generator," *Gas Turbines Power,* vol. 136, no. 3, 2013.

[15] Keun Ryu, Luis San Andres, "On the Failure of a Gas Foil Bearing: High Temperature Operation Without Cooling Flow," *Gas Turbines Power,* vol. 135, no. 11, 2013.

[16] H. Heshmat, "Advancedments in the Performance of Aerodynamic Foil Journal Bearings High Speed and Load Capacity," *Journal of Tribology,* pp. 284-295, 1994.

[17] Iordanoff, "Analysis of an Aerodynamic Compliant Foil Thrust Bearing: Method for a Rapid Design," *Journal of Tribology,* vol. 121, no. 4, pp. 816-822, 1999.

[18] H. Heshmat, "Major breakthrough in Load Capacity, Speed and Operating Temperature of Foil Thrust Bearings," World Tribology Congress, 2008.

[19] San Andres, Keun Ryu, "Prediction of Gas Thrust Foil Bearing Performance for Oil-Free Automotive Turbochargers," *Gas Turbines Power,* vol. 137, no. 3, 2014.

[20] Z. C. Peng, M. M. Khonsari, "Hydrodynamic Analysis of Compliant Foil Bearinngs with Compressible Air Flow," *Journal of Tribology,* vol. 126, no. 3, pp. 542-546, 2004.

[21] Z.C. Peng, M. M. Khonsari, "On the Limiting Load-Carrying Capacity of Foil Bearings," *Journal of Tribology,* vol. 4, no. 126, pp. 817-818, 2004.

[22] R.N. Ravikumar, K.J. Rathanraj, "Comparative Experimental Analysis of Load Carrying Capability of Air Foil Thrust Bearing for Different Configuration of Foil Assembly," *Procedia Technology,* vol. 1, no. 25, pp. 1096-1105, 2016.

[23] Daejong Kim, Soongkook Park, "Hydrostatic Air Foil Bearings: Analytical and Experimental Investigation," *Tribology International,* vol. 42, no. 3, pp. 413-425, 1009.

[24] Manish Kumar, Daejong Kim, "Static performance of hydrostatic air bump foil bearing," *Tribology International,* vol. 43, no. 4, pp. 752-758, 2010.

[25] S. Bauman, "An Oil-Free Thrust Foil Bearing Facility Design, Calibration, and Operation," NASA, Cleveland, 2005.

[26] Donghyun Lee, Daejong Kim, "Design and Performance Prediction of Hybrid Air Foil Thrust Bearings," *Gas Turbines Power,* vol. 133, no. 4, 2010.

[27] D. Kim, *Tribology Notes,* Arlington: The University of Texas at Arlington, 2015.

[28] Zhiqiang Liu, Meng Hua, "Wear transitions and mechanisms in lubricated sliding of a molybdenum coating," *Tribology International,* vol. 32, no. 9, pp. 499-506, 1999.

[29] "Molybdenum Disulfide Coatings (MoS2 Coatings)," Metal Coatings, [Online]. Available: https://www.metcoat.com/molybdenum-disulfide-coatings.htm.

[30] Adolofo Delgado, Bugra Ertas, "Dynamic Force Coefficients of Hydrostatic Gas Films for Recessed Flat Plates: Experimental Identification and Analytical Predictions," *Journal of Tribology,* vol. 140, no. 6, 2018.

[31] H.M. Talukder, T.B. Stowell, "Pneumatic hammer in an externally pressurized orifice-compensated air journal bearing," *Tribology International,* vol. 36, no. 2, pp. 585-591, 2003.

[32] J. Egolf, Air Bearing Optimization.

[33] R.J.Bruckner, "Performance of Simple Gas Foil Thrust Bearings in Air," Supercritical CO2 Power Cycle Symposium, Cleveland, 2012.

[34] Zhiyang Guo, Lyu Peng, Kai Feng, Wanhui Liu, "Measurement and prediction of nonlinear dynamics of a gas foil bearing supported rigid rotor system," *Measurement,* vol. 121, pp. 205-217, 2018.

[35] Kevin Radil, Samuel Howard, Brian Dykas, "The Role of Radial Clearance on the Performance of Foil Air Bearings," *Tribology Transactions,* vol. 45, no. 4, pp. 485-490, 2002.

[36] Kai Feng, Han-Quing Guan, Zi-Long Zhao, Tian-Yu Liu, "Active bump-type foil bearing with controllable mechanical preloads," *Tribology International,* vol. 120, pp. 187-202, 2018.

[37] J. Shi, Hydrodynamic Lubrication Analysis of a Foil Journal Bearing: Pressure and Lift Build-up, UTRC.

Biographical Information

Myongsok Song graduated with a Bachelor's Degree in Mechanical Engineering from Hanyang University in Seoul, South Korea, in 2015. He joined the University of Texas at Arlington to pursue a Master's degree in Mechanical Engineering in fall 2016.

Address: Department of Mechanical and Aerospace Engineering, Woolf Hall, Room 211, Box 19023, Arlington, TX 76019

Email Address: myongsoksong@outlook.com